

---

Electronic Thesis and Dissertation Repository

---

5-23-2022 10:00 AM

# The Hydrophobic Residues in Amino Terminal Domains of Cx46 and Cx50 are Important for their Gap Junction Channel Ion Permeation and Gating

Roa'a Jaradat, *The University of Western Ontario*

Supervisor: Bai, Donglin, *The University of Western Ontario*

A thesis submitted in partial fulfillment of the requirements for the Master of Science degree in Physiology and Pharmacology

© Roa'a Jaradat 2022

Follow this and additional works at: <https://ir.lib.uwo.ca/etd>



Part of the [Biophysics Commons](#), and the [Cellular and Molecular Physiology Commons](#)

---

## Recommended Citation

Jaradat, Roa'a, "The Hydrophobic Residues in Amino Terminal Domains of Cx46 and Cx50 are Important for their Gap Junction Channel Ion Permeation and Gating" (2022). *Electronic Thesis and Dissertation Repository*. 8553.

<https://ir.lib.uwo.ca/etd/8553>

This Dissertation/Thesis is brought to you for free and open access by Scholarship@Western. It has been accepted for inclusion in Electronic Thesis and Dissertation Repository by an authorized administrator of Scholarship@Western. For more information, please contact [wlsadmin@uwo.ca](mailto:wlsadmin@uwo.ca).

## Abstract

Connexins are ubiquitous transmembrane proteins that assemble to form intercellular channels, called gap junctions (GJs). The amino terminal (NT) domain and residues within this domain have been shown to be important for both  $V_j$ -gating and single channel conductance ( $\gamma_j$ ) of several GJs including Cx46 and Cx50. High-resolution structures of Cx46 and Cx50 GJs were recently resolved showing that NT domain folds into the inner pore where hydrophobic residues are packed against M1/2 domains stabilizing open-state conformation. We studied functional properties of GJs formed by several point variants at NT (Cx46 L10I, N13E, A14V, Q15N and Cx50 I10L, E13N, V14A, N15Q) and M2 domain (Cx50 S89T) in GJ-deficient N2A cells. We found that these variants formed functional GJs except Cx50 S89T. Altered coupling conductance,  $\gamma_j$ , and/or  $V_j$ -gating observed in GJs of L10I and A14V indicate these hydrophobic residues are important for  $V_j$ -gating and  $\gamma_j$  of these and possibly other GJs.

## Keywords

Gap junction, connexin, voltage gating, conductance, patch clamp.

## Summary for Lay Audience

Our body cells communicate via various mechanisms to maintain organ functioning and tissue homeostasis. One of these mechanisms is gap junction channels (GJs), which is composed of 12 connexin proteins, mediating transfer of ions and other molecules between two adjacent cells. Connexins vary in amino acids composition and thus makes different GJs with unique properties. One part of the connexin, called amino terminal (NT) domain, folds in the channel pore acting as a physical barrier to the permeating ions and molecules. Changing the amino acid composition of the NT domain had been shown to alter channel properties. However, how NT domain regulates channel function is still not fully determined. Recent structural studies provided novel high-resolution structure models of lens connexin46 and connexin50 gap junctions. The new structures indicate that NT domain is anchored to other domains via a few NT amino acid residues showed hydrophobic properties, including those at 10<sup>th</sup> and 14<sup>th</sup> positions in these two connexins. To test these and other different amino acid residues in these lens connexins on their gap junction properties, we studied the effect of switching these residues one at a time on its gap junction permeation and opening/closing controls. Our results indicate that hydrophobic residues in the NT domain could also play an important role in control gap junction ion permeation and open/close regulation as suggested by the structure models. Our study combines structural and functional studies to illustrate the mechanisms of how the NT domain shapes channel properties in these gap junction channels.

## Co-Authorship Statement

Chapter 2 will be submitted as a manuscript for publication. Roa'a Jaradat designed and performed all patch clamp experiments, analyzed data, and wrote an early draft of the manuscript. Honghong Chen designed and generated all variants. Peter Stathopoulos developed homology structure models. Donglin Bai designed the project, supervised data analysis, acquired funding, and critically revised the manuscript

## Acknowledgments

This project would not have been accomplished without the support of many people. I would like to thank my supervisor, Dr. Donglin Bai, for his patience, guidance, and invaluable insights leading to the writing of this thesis. Thanks to Honghong Chen for her continuous help and guidance. Also, thanks to my committee members, Drs. Brian Shilton, Lina Dagnino, and Peter Stathopoulos who provided many helpful comments and suggestions. It was a pleasure to work with Benny Yue (former student), Tianhe Li, and Robert Wong, your company in the laboratory will be always remembered. Many thanks to my parents, husband and kids who endured this long process with me, always offering support and love.

# Table of Contents

Abstract.....	ii
Keywords .....	ii
Summary for Lay Audience.....	iii
Co-Authorship Statement.....	iv
Acknowledgments .....	v
Table of contents .....	vi
Abbreviations.....	viii
List of figures and tables.....	x
Chapter 1.....	1
1 Gap junction channels.....	1
1.1 Connexins .....	1
1.2 The NT domain.....	3
1.3 Voltage regulation of GJ channels.....	4
1.4 Single channel properties.....	5
1.5 Lens connexins.....	5
1.6 Rationale and hypothesis .....	10
1.7 Objectives .....	12
1.8 Refernces.....	13
Chapter 2.....	19
2 Manuscript .....	19
2.1 Abstract.....	19
2.2 Introduction.....	20
2.3 Materials and methods .....	24
2.3.1 Plasmid construction .....	24

2.3.2 Cell culture and transient transfections .....	25
2.3.3 Electrophysiological recording .....	25
2.3.4 Transjunctional voltage dependent gating .....	26
2.3.5 Single channel analysis .....	27
2.3.6 Homology structure modeling and electrostatic analysis.....	27
2.3.7 Statistical analysis .....	27
2.4 Results.....	28
2.4.1 Homotypic Cx46 and Cx50 variants form functional GJ channels.....	28
2.4.2 $V_j$ -gating properties of homotypic Cx46, Cx50, and variant GJ channels.....	31
2.4.3 Unitary channel properties of homotypic Cx46, Cx50, and vriant GJ channels .....	39
2.5 Homology modeling of selected Cx46 and Cx50 variants .....	44
2.5 Discussion.....	49
2.6 References.....	54
Chapter 3.....	59
3.1 Overall study.....	59
3.2 Sequence alignment and design of variants .....	59
3.3 Functional characterization of NT variants of Cx46 and Cx50 GJs .....	61
3.4 Comparison among human, sheep, and mouse lens GJs .....	65
3.5 Limitations and future studies.....	65
3.6 Summary .....	65
3.7 References .....	68
Curriculum Vitae .....	71

## Abbreviations

<b>A</b>	Measure of $V_j$ -gating sensitivity in Boltzmann equation
<b>CL</b>	Cytoplasmic loop of a connexin
<b>Cryo-EM</b>	Cryogenic Electron Microscopy
<b>CT</b>	Carboxyl-terminus of a connexin
<b>Cx46</b>	Connexin46
<b>Cx50</b>	Connexin50
<b>DMEM</b>	Dulbecco's Modified Eagle's medium
<b>EGTA</b>	Ethylene glycol-bis ( $\beta$ -aminoethyl ether)-N,N,N',N'-tetraacetic acid
<b>E1</b>	The first extracellular loop domain of a connexin
<b>E2</b>	The second extracellular loop domain of a connexin
<b>ECS</b>	Extracellular solution
<b>FBS</b>	Fetal bovine serum
<b>GFP</b>	Green fluorescent protein
<b>G<sub>max</sub></b>	Maximum normalized conductance in Boltzmann equation
<b>G<sub>min</sub></b>	Minimum normalized conductance in Boltzmann equation
<b>GJ</b>	Gap junction
<b>G<sub>j</sub></b>	Transjunctional conductance
<b>G<sub>j,ss</sub></b>	Normalized steady state transjunctional conductance



<b>HEPES</b>	4-(2-hydroxyethyl)-1-piperazineethanesulfonic acid
<b>ICS</b>	Intracellular solution
<b>I<sub>j</sub></b>	Gap junctional current
<b>i<sub>j</sub></b>	Unitary gap junctional current
<b>kDa</b>	Kilo Dalton
<b>M1 – M4</b>	Transmembrane domain 1 – 4 of a connexin
<b>mV</b>	Millivolts
<b>N2A</b>	Mouse neuroblastoma cells
<b>nS</b>	Nanosiemens
<b>NT</b>	Amino terminus
<b>ODDD</b>	Oculodentodigital dysplasia
<b>pIRES</b>	Plasmid containing internal ribosome entry site
<b>P<sub>open</sub></b>	Open probability
<b>pS</b>	Picosiemens
<b>SD</b>	Standard deviation
<b>V<sub>0</sub></b>	Voltage at which the conductance is half between the maximum and minimum
<b>V<sub>j</sub></b>	Transjunctional voltage
<b>γ<sub>j</sub></b>	Gap junction unitary channel conductance

## List of Figures and Tables

Figure 1-1: Gap junction structure and nomenclature..	2
Figure 1-2: Cellular structure of the lens .....	7
Figure 2-1: The NT domains of Cx26 and Cx46 are different in spatial orientations with respect to the transmembrane domains (M1 and M2).....	23
Figure 2-2: Amino acid sequence alignment of sheep Cx46 and Cx50.....	23
Figure 2-3: Coupling percentage and conductance ( $G_j$ ) of N2A cell pairs expressing homotypic wildtype Cx46, Cx50, and their variants on 10 <sup>th</sup> , 13 <sup>th</sup> , 14 <sup>th</sup> , and 15 <sup>th</sup> positions in the NT domain as indicated.....	30
Figure 2-4: $V_j$ -gating of homotypic Cx46, Cx50 gap junction channels. ....	33
Figure 2-5: $V_j$ -gating properties of GJs formed by Cx46 variants, L10I, N13E, A14V, and Q15N.....	35
Figure 2-6: $V_j$ -gating properties of the GJs formed by Cx50 variants, I10L, E13N, V14A, or N15Q.....	37
Figure 2-7: Unitary channel properties for wildtype Cx46 and Cx50 GJs .....	41
Figure 2-8: Single channel currents ( $i_{js}$ ) recorded in response to the indicated $V_{js}$ . ....	43
Figure 2-9: Unitary channel properties of homotypic GJs of Cx46 L10I, N13E, A14V, Q15N and Cx50 I10L, E13N, V14A, N15Q variants.....	44
Figure 2-10: Structural models for selected variant GJs.....	48
Figure 2-11: Cx50 S89T failed to form functional GJs. ....	49
Figure 3-1: Sequence alignment of sCx46 and sCx50 at the NT domain.....	62

**Figure 3-2:** Sequence logos of the first 20 amino acid residues in the amino terminal domains (left hand is the beginning of amino terminus) of Cx46, Cx50, and their orthologs are shown... 64

Table 2-1: Boltzmann fitting parameters for the GJs of Cx46 and its variants. .... 38

Table 2-2: Boltzmann fitting parameters for the GJs of Cx50 and its variants. .... 39

Table 3-1: Summary of functional changes observed in each variant as compared to corresponding Cx46 or Cx50 wildtypes. .... 66

# Chapter 1

## 1 Gap Junction Channels

Gap junctions (GJs) are large-diameter channels facilitating the direct passage of ions, nutrients, metabolites, and small molecules up to 1 kDa between adjacent cells. Beside chemical coupling, GJs also allow cells to electrically couple via the transfer of ions such as,  $K^+$ ,  $Na^+$ ,  $Cl^-$ , and  $Ca^{2+}$ . This fast communication is especially important in the conduction of action potential in cardiac contractions and neuronal activities (Goodenough and Paul, 2009, Evans and Martin, 2002, Nielsen et al., 2012). It is well established that GJs contribute to the maintenance of physiological processes across many tissues through the study of gene mutations in humans and rodents as well as gene knockouts in mouse models (Dobrowolski and Willecke, 2009, Simon and Goodenough, 1998, Zoidl and Dermietzel, 2010). Dysfunction of GJs can hinder cellular communication and lead to a plethora of pathophysiological conditions, including neurological disorders, cardiovascular disease, blindness, deafness, and cancers (Vinken et al., 2003). Each GJ channel is formed by the docking of two hexameric assemblies, named hemichannels or connexons, of integral membrane proteins called connexins (Foote et al., 1998, Evans et al., 1999). A hemichannel can be homomeric or heteromeric if it has same or different connexin proteins, respectively, while GJs can be homotypic if they are composed from the same homomeric hemichannels, or heterotypic otherwise (Bai and Wang, 2014) as depicted in Fig. 1-1. Tissue cells commonly express one or more connexins. Thereby, cells can express diverse homo- or heterotypic GJs that consequently finely tune diverse functions across the tissue.

### 1.1 Connexins

The connexin gene family includes 21 members in the human genome which display distinct tissue distribution, while each tissue commonly expresses more than one connexin protein. To illustrate, Cx43, Cx46, and Cx50 are expressed in human eye lens while Cx36, Cx45, and Cx62 are present throughout the nervous system (Willecke et al., 2002, Söhl et al., 2005). Despite that connexins exhibit variable properties and tissue

expression, all are predicted to share similar structural topology consisting of four transmembrane domains (M1-M4) connected by two extracellular loops (E1 and E2) and one cytoplasmic loop (CL) alongside the cytosolic amino and carboxyl termini (NT and CT, respectively) (Goodenough and Paul, 2009) as illustrated in Fig. 1-1.

Transmembrane domains, extracellular loops, and the NT domain show high conservation level among connexins as opposed to the CL as well as CT domains which are highly variable in terms of length and amino acid sequence (Abascal and Zardoya, 2013). The number shown in connexin protein nomenclature represents molecular mass in kilodaltons theoretically calculated from the protein sequences (Vinken, 2015). Genes that encode connexins are classified into five groups:  $\alpha$ ,  $\beta$ ,  $\gamma$ ,  $\delta$ , and  $\epsilon$  based on the sequence similarity. Genes are denoted GJ followed by a letter and a number to denote family and order of discovery. To illustrate, *GJA8* corresponds to the 8th gene in the alpha family according to order of discovery, respectively, and it encodes Cx50 protein (Söhl and Willecke, 2004).

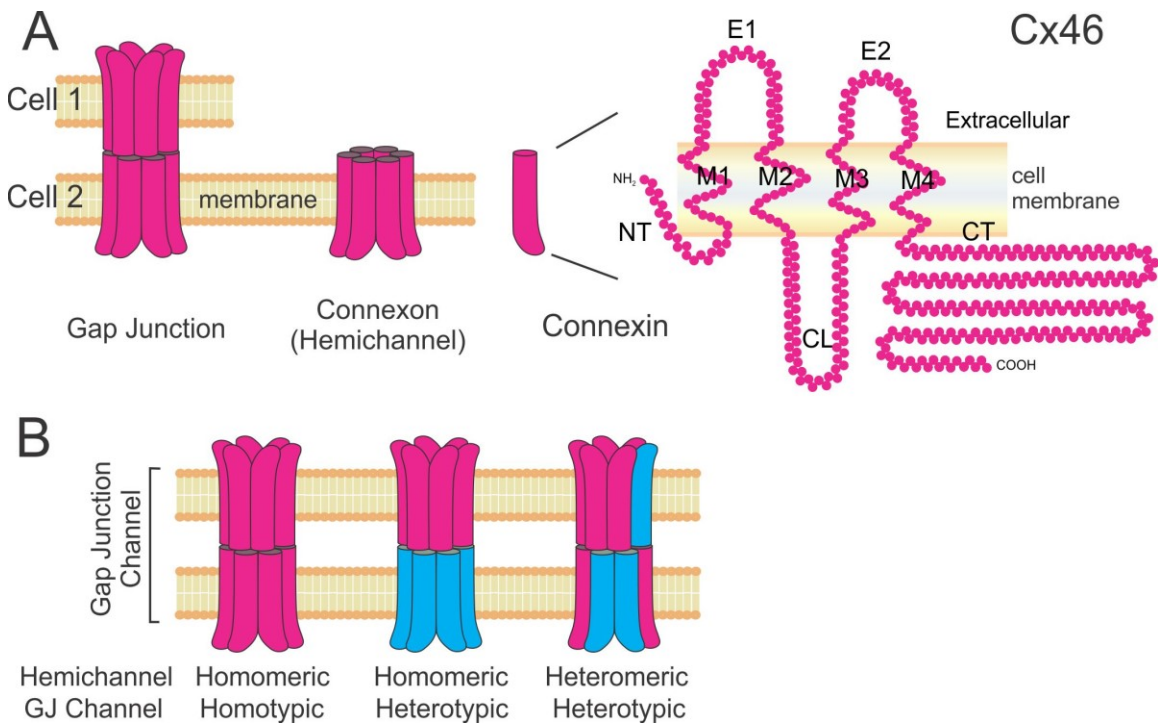


**Figure 1-1:** Modified figure from (Bai et al., 2018).

## 1.2 The NT domain

Each connexin domain serves a unique function to its GJ channel. Residues within the NT domain have been shown to play an important role in determining the gating polarity and channel properties such as transjunctional voltage ( $V_j$ )-dependent gating ( $V_j$ -gating) and single channel conductance ( $\gamma_j$ ) in several connexins (see below) (Verselis et al., 1994, Purnick et al., 2000, Musa et al., 2004, Peracchia and Peracchia, 2005, Kronengold et al., 2012). Previous studies explored the role of the charged residues in the NT domain of Cx46, Cx50, or their orthologues, especially residues at the very beginning part of NT, demonstrated that they control gating polarity, channel pore open stability, and single channel conductance of these GJ channels (Musa et al., 2004, Peracchia and Peracchia, 2005, Xin and Bai, 2013, Tong and Ebihara, 2006). However, previous functional studies which exchanged charged residues with others of similar charge properties (such as D3E in Cx50 and R9K in Cx45) resulted in significant changes in channel  $V_j$ -gating properties or  $\gamma_j$ , suggesting a role for additional factor(s) other than charge as important determinants of GJ functional properties (Santos-Miranda et al., 2020, Xin et al., 2012).

The first high resolution (3.5 Å) crystal structure was resolved for human Cx26 GJ where the NT domains of the 6 subunits of each hemichannel were shown to form a funnel structure comprising the narrowest part of the GJ (Maeda et al., 2009). Thereby, the NT domain acts as a structural determinant of molecular size restriction at the channel vestibule. Later, single particle cryo-electron microscopy (Cryo-EM) was used to resolve the structure of native sheep Cx46 and Cx50, at 3.4 Å resolution, showing that the NT domain also adopts an  $\alpha$ -helix that folds into the channel vestibule (Myers et al., 2018). These structural findings align well with previously identified important functional role of the NT domain. Different from the Cx26 GJ structure, the structures of Cx46 and Cx50 GJ showed that the NT domain adopts a regular amphipathic  $\alpha$ -helical structure (see Fig. 2-1), of which the hydrophobic residues of the NT domain packed against the other pore lining M1 and M2 domains stabilizing the conformation of GJs while the hydrophilic residues are facing the pore and are likely involved in  $V_j$  sensing, regulating ion or substrate selectivity, and the rate of ion or substrate permeation (Myers et al., 2018, Flores et al., 2020).

### 1.3 Voltage Regulation of GJ Channels

Gap junction channels can be gated via various mechanisms, such as intracellular divalent cations ( $\text{Ca}^{2+}$  and  $\text{Mg}^{2+}$ ), pH changes, and transjunctional voltage ( $V_j$ ) (Spray et al., 1981). Transjunctional voltage ( $V_j$ ) is the electric potential difference between the interior of two coupled cells (Oh and Bargiello, 2015). Transjunctional voltage ( $V_j$ ) dependent gating ( $V_j$ -gating) describes how the amplitude of the macroscopic junctional current ( $I_j$ ) decline with time during a constant  $V_j$  pulse commonly observed at high  $V_j$ s ( $\pm 40$ -100 mV) dependent on the composed connexins. Most connexins show little gating at low  $V_j$ s ( $\pm 10$ -20 mV).  $V_j$ -gating is a distinct property for each GJ channel as the rate (kinetics) and extent can vary. Molecular determinants underlying  $V_j$ -gating appear to be different among GJs of different connexins as some studies on Cx26 and Cx32 GJs proposed conformational changes that change location of voltage sensor in the NT domain (Bargiello et al., 2012, Oh et al., 2000). In contrast, other mechanism shown by studies on Cx40 and Cx43 GJs suggests that the CT could act as a gating particle binding to a receptor in the CL to close the GJ pore (Anumonwo et al., 2001, Moreno et al., 2002).

The development of dual whole-cell voltage clamp technique has enabled researchers to measure electrophysiological properties such as  $V_j$ -gating and unitary channel conductance ( $\gamma_j$ ) (Spray et al., 1981). This technique offers many advantages as it enables accurate measurement of the coupling conductance and allows for flexible control of the  $V_j$  (Bai and Cameron, 2016). Gap junction-deficient model cells, such as mouse neuroblastoma N2A cells, human cervical carcinoma HeLa cells, and rat insulinoma cells (RIN), are frequently used as vehicle to express connexins of interest to study their electrophysiological properties (Cottrell and Burt, 2001, Bai et al., 2006, Valiunas, 2002). Briefly, an isolated cell pair is patched by micropipettes in whole cell voltage clamp mode. A series of voltage pulses is administered ranging from  $\pm 20$  to  $\pm 100$  mV on pulsing cell and the other cell (recording cell) held at a steady voltage of 0 mV. If functional GJs exist between the patched cell pair, the recording cell will display  $I_j$ s in response to the various  $V_j$ s. Coupling conductance ( $G_j$ ) can be then calculated via the equation ( $G_j = I_j/V_j$ ).

Macroscopic current recordings, obtained from cell pairs expressing multiple GJ channels, can be used to measure the amplitudes of  $I_j$  peak that gradually deactivates to reach a steady state usually near the end of the  $V_j$  pulse (at high  $V_j$ s,  $\pm 40$  to  $\pm 100$  mV). The steady state  $G_j$  is normalized to the peak  $G_j$  to obtain a normalized steady-state junctional conductance ( $G_{j,ss}$ ), which can be plotted with the entire tested  $V_j$  range. This  $G_{j,ss} - V_j$  relationship can be quantitatively described by a two-state Boltzmann equation (Spray et al., 1981).

## 1.4 Single channel properties

Single GJ channel currents ( $i_j$ s) can be observed in low coupled cell pairs with few GJ channels. Single GJ channel currents can provide detailed information on channel properties such as, main unitary channel conductance ( $\gamma_j$ ), residue conductance (or subconductance,  $\gamma_{j,sub}$  or  $\gamma_{j,res}$ ), probability of open, residue, and closed state ( $P_{open}$ ,  $P_{res}$  or  $P_{sub}$  and  $P_{closed}$ , respectively), and open dwell time (Tong et al., 2014, Xin et al., 2012, Xin et al., 2010, Yue et al., 2021). Unitary channel conductance varies dramatically among connexin gap junction channels, ranging from 300 pS for Cx37 (Veenstra et al., 1994) to only 5-15 pS in Cx36 homotypic GJs (Moreno et al., 2002, Srinivas et al., 1999, Teubner et al., 2000). Although molecular determinants of  $\gamma_j$  are still not fully elucidated, physical pore size and pore surface electrostatic potential have been shown to affect  $\gamma_j$ . To illustrate, increasing the net negative charge of the NT domain in several positions was associated with an increase in  $\gamma_j$ , while increasing positive charges reduced  $\gamma_j$  (Xin and Bai, 2013, Tejada et al., 2018). Most studied GJ channels display single channel currents that show different conductance states: the main open state, sub-conducting (also known as residue) state or substate, and a fully closed state (Bukauskas and Verselis, 2004, Bukauskas and Weingart, 1994).

## 1.5 Lens connexins

The eye lens maintains normal vision by focusing the light onto the retina. Thereby, it must be transparent to fulfill this role. Because blood vessels can scatter or absorb light, the lens lacks vasculature and is dependent on its internal micro-circulatory system, maintained partly by GJs, to obtain nutrients and remove metabolic wastes (Mathias et



al., 2010). Moreover, mature fiber cells, which constitute most of the lens body, lack nuclei and organelles to prevent light scattering. Lens epithelium is the second type of lens cells which markedly differ in morphology compared to fiber cells (Fig. 1-2). They form an anterior layer of nucleated cells that facilitate active transport and metabolic activities within the lens (Beyer et al., 2013, Mathias et al., 2010). At the epithelium surface,  $\text{Na}^+\text{-K}^+\text{-ATPases}$  play a critical role to maintaining ion gradients necessary for lens circulation. Fiber cell GJs and  $\text{Na}^+$  channels are crucial components of the lens circulation system. The lens is bathed and nourished by aqueous humor, which is a dynamic water-like liquid that maintains lens homeostasis and fiber cell resting membrane potential by supplying oxygen and nutrients and removing metabolic wastes and carbon dioxide (Goel et al., 2010). Because the lens fiber cell resting membrane potential is around -70 mV, there is a significant electrochemical gradient for  $\text{Na}^+$  to enter the lens cells through  $\text{Na}^+$  channels. Although these channels have limited permeability, fiber cells are numerous; thus, the result is a huge  $\text{Na}^+$  influx from extracellular space into fiber cells. Subsequently the  $\text{Na}^+$  passes from one fiber cell to another via GJs until it reaches the epithelium where  $\text{Na}^+\text{-K}^+\text{-ATPase}$  excretes the  $\text{Na}^+$  from intracellular to extracellular fluid. The molecular identity of fiber cell  $\text{Na}^+$  channels is still unknown with a presumption that  $\text{Na}^+$  influx might be through hemichannels (Mathias et al., 2007).

At the lens equator, epithelial cells differentiate into fiber cells. During maturation process, fiber cells lose their nuclei and organelles and synthesize high concentration of soluble crystallins, to maintain transparency and a high refractive index that are essential for clear vision (Mathias et al., 2010). Epithelial cells express both Cx43 and Cx50 while fiber cells abundantly express Cx46 and Cx50. Because GJs formed by each connexin have distinct gating and permeation characteristics, and Cx46 was demonstrated to co-oligomerize with both Cx43 and Cx50, the eye lens can express different heterotypic GJs allowing for functional diversity that helps this avascular organ fulfill its physiological role (Jiang and Goodenough, 1996, White et al., 1994).

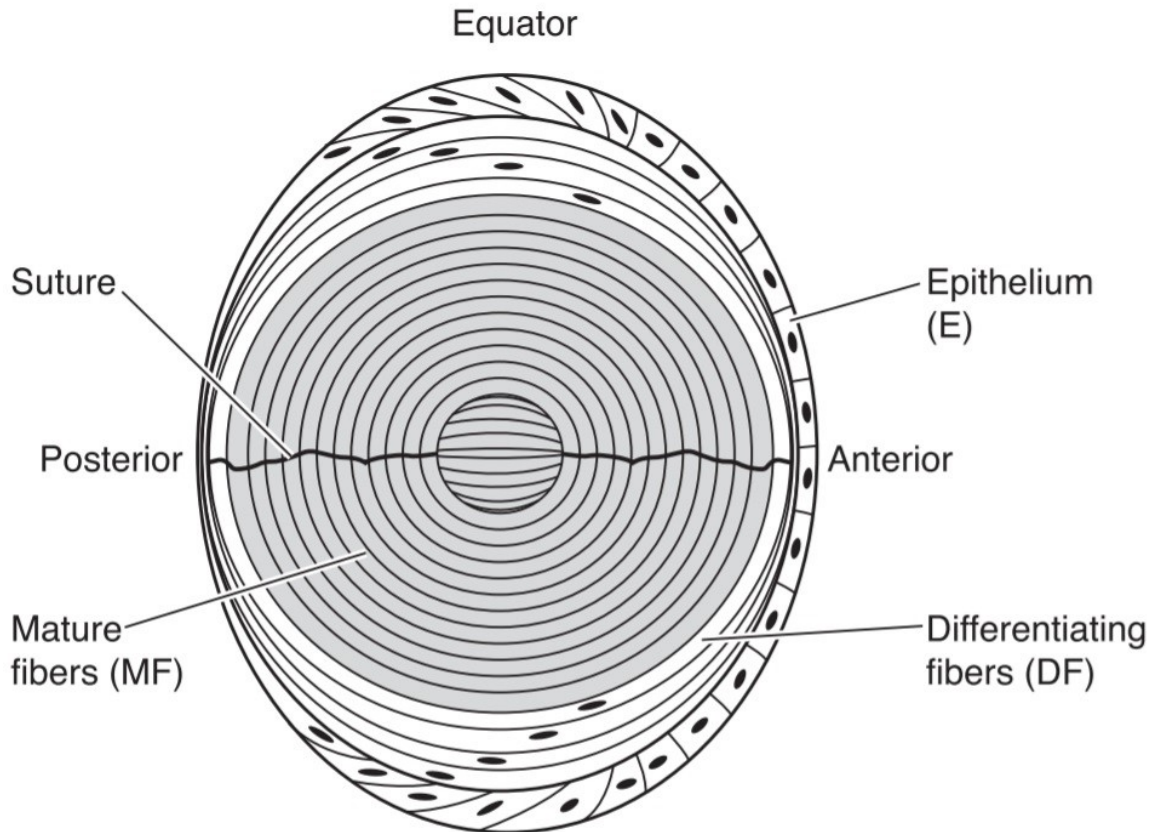


**Figure 1-2:** Cellular structure of the lens: Epithelial cells (E) which forms a layer at the anterior surface of lens, differentiating fibers (DF) which extends from the surface to 15% towards the core, and the mature fibers (MF) which lacks organelles and fill in the majority of lens body. Modified from (Mathias et al., 2010). Lens equator is the boundary between the lens epithelium and the lens fiber core where epithelial cells differentiate into fiber cells. Lens suture refers to the overlap between lens fiber cell ends anteriorly and posteriorly.

Cataracts are the presence of cloudy or opaque regions in the eye lens obscuring the transmission of light to the retina. The transmission of light is essential to maintain clear vision. Cataracts are considered the leading cause of blindness worldwide (Rao et al., 2011). Mutations in *GJA3* and *GJA8*, the two genes encoding Cx46 and Cx50 respectively, cause 15% of hereditary cataracts, primarily inherited as autosomal dominant traits (Shiels and Hejtmancik, 2013). A total of 116 congenital cataract-linked variants of Cx46 and Cx50 have been identified with approximately 40% of these

variations localized in the NT, M1, or M2 domains (Bai et al., 2021). Consistent experimental evidence from knock-out (KO) and knock-in (KI) animal models has revealed that both Cx46 and Cx50 are implicated in cataract pathogenesis (Gong et al., 1997, Rong et al., 2002). However, the cataract type and onset time is different. For example, Cx50 KO mice showed mild nuclear cataracts that don't deteriorate with time concomitant with a reduction in lens mass by 46%. This reduction in lens mass is called microphthalmia. Cx46 KO resulted in severe nuclear cataracts that progressively worsened with age; however, lens size was not affected (White et al., 1998, Gong et al., 1997, Rong et al., 2002). Cx50 is believed to contribute to lens cell proliferation because replacement of the Cx50 coding region with that of Cx46 (Cx50<sup>46/46</sup> KI) mice did not fully rescue the normal mitotic index (Sellitto et al., 2004, White, 2002). However, these Cx50<sup>46/46</sup> KI mice did not develop cataracts suggesting a role of Cx46 in cellular differentiation.

On the other hand, the role of Cx43 in lens function is controversial. Lenses of Cx43 KO mouse embryos appeared normal and transparent (White et al., 2001); however, other studies found separations between epithelial cells as well as between epithelial and fiber cells with extracellular spaces and intracellular vacuoles in the lenses of these mice suggesting a role for Cx43 in epithelial-fiber cell communication (Gao and Spray, 1998). Since Cx43 KO is lethal to neonatal mice, long term effects cannot be assessed (Reaume et al., 1995). Nevertheless, conditional deletion of Cx43 did not cause cataracts, and lenses appeared normal until at least 6 months of age (DeRosa et al., 2009). Moreover, Cx43 appears to be essential to produce normal aqueous humor (Calera et al., 2006). Specific mutations in Cx43 gene cause an autosomal dominant disorder called oculodentodigital dysplasia (ODDD) which affects different tissues including the eye. Ocular -related findings associated with Cx43 mutations include microphthalmia, microcornea, iris malformation, cataracts, elevated intraocular pressure, and glaucoma (Frasson et al., 2004, Loddenkemper et al., 2002, Musa et al., 2009, Doshi et al., 2016).

To sum up, each of the three lens connexins (Cx50, Cx46, and Cx43) is specifically tailored to serve a function in the lens. Collectively, these connexins maintain lens homeostasis and function. Knocking out genes encoding Cx46 and Cx50 result in a

specific form of cataract (mild or severe) or development of early stage of cataracts in mice. More than one hundred mutations in human genes encoding Cx46 and Cx50 have been linked to congenital cataracts.

## 1.6 Rationale and Hypothesis

Structure-function studies are required to gain mechanistic insights into molecular determinants for GJ gating and the rate of ion permeation after the provision of a high resolution cryo-EM structure of native sheep Cx46 and Cx50 at 3.4 Å resolution (Myers et al., 2018) and more recently at 1.9 Å resolution (Flores et al., 2020). These GJ structures are the first to reveal that the NT domain adopts an amphipathic  $\alpha$ -helix in which the hydrophobic amino acids are packed against the other pore lining M1 and M2 domains, stabilizing the NT domain in a GJ channel open conformation. Moreover, a previous study from our lab showed that switching the NT domain of Cx46 with that of Cx50 (Cx46-50NT) resulted in a nonfunctional GJ channel, while switching the NT domain of Cx50 with that of Cx46 resulted in forming functional GJs but without much  $V_j$ -gating and a reduced single channel conductance ( $\gamma_j$ ). The roles of individual NT residues in these two lens connexins are unclear in terms of functional status,  $V_j$ -gating properties, and  $\gamma_j$ . Our initial attempt identified that the R9 in Cx46 and N9 in Cx50 play a role in determining  $\gamma_j$  and  $V_j$ -gating (Yue et al. 2021). To identify the individual NT residues in their role in regulating  $V_j$ -gating and ion permeation, we designed four pairs of missense variants in either Cx46 or Cx50 NT domain (for details see below) and studied their functional status by checking both the coupling percentage and coupling conductance as well as  $V_j$ -gating properties and  $\gamma_j$ . We also developed homology structure models based on Cx46 and Cx50 GJ structures to evaluate those residues in M1 or M2 of the same or neighboring subunits capable to have close interact with the NT residues, especially those hydrophobic residues. Our results and homology models indicate an important role of hydrophobic residues in the NT domain, which interact with M1 and/or M2 to stabilize the NT domain in the open conformation. Steric clash in mutations on hydrophobic residues could lead to impaired GJ function or severely alter  $\gamma_j$  or  $V_j$ -gating. Our study is the first to identify that individual hydrophobic NT residues in Cx46 and Cx50 GJ are important for functional status,  $V_j$ -gating properties, and single channel conductance. Given that the hydrophobic residues are highly conserved in Cx46 and Cx50 and also in related and non-related connexin families, they are likely to play a similar role in other GJs, i.e., to stabilize the NT domain in an open conformation.

We hypothesized that  $V_j$ -gating and  $\gamma_j$  of Cx46 and Cx50 GJs are mediated in part by their hydrophobic residues (at 10<sup>th</sup> and 14<sup>th</sup> positions of NT domain) by interacting with M1 and/or M2 domains altering the stability of the open state conformation. We also hypothesized that the increase in the size of amino acid side chain (N13E, A14V, N15Q, S89T) will introduce steric hinderance affecting functional status,  $V_j$ -gating properties, and/or  $\gamma_j$ .

## 1.7 Objectives

To contribute to the understanding of the structure-function relations, highlight the role of hydrophobic residues interactions, and identify the role of different side chains' properties, we investigated functional properties ( $\gamma_j$  and  $V_j$ -gating) of homotypic GJs formed by sheep connexins, Cx46 and Cx50, and their point variants, especially near the pore entrance area, at the 10<sup>th</sup> (Cx46 L10I, Cx50 I10L), 13<sup>th</sup> (Cx46 N13E, Cx50 E13N), 14<sup>th</sup> (Cx46 A14V, Cx50 V14A), and 15<sup>th</sup> (Cx46 Q15N, Cx50 N15Q) residues as well as in the M2 domain (Cx50 S98T) in gap junction deficient mouse neuroblastoma cells (N2A cells) via dual whole-cell voltage clamp technique. Our specific objectives are as follows:

- i. To study the coupling percentage and coupling conductance of the following point variants at the 10<sup>th</sup>, 13<sup>th</sup>, 14<sup>th</sup>, and 15<sup>th</sup> positions of NT (Cx46 L10I, N13E, A14V, Q15N and Cx50 I10L, E13N, V14A, N15Q) and M2 domains (Cx50 S89T).
- ii. To characterize  $V_j$ -gating properties of GJs formed by each of these variant GJs.
- iii. To determine single channel conductance ( $\gamma_j$ ) of GJs formed by each of these variant GJs.
- iv. To generate homology models of selected variants to see changes on non-covalent intra- or inter-subunit interactions, which could provide structural mechanistic insights on their unique GJ properties.

## 1.8 References:

- ABASCAL, F. & ZARDOYA, R. 2013. Evolutionary analyses of gap junction protein families. *Biochim. Biophys. Acta*, 1828, 4-14.
- ANUMONWO, J. M., TAFFET, S. M., GU, H., CHANSON, M., MORENO, A. P. & DELMAR, M. 2001. The carboxyl terminal domain regulates the unitary conductance and voltage dependence of connexin40 gap junction channels. *Circ. Res.*, 88, 666-73.
- BAI, D. & CAMERON, J. A. 2016. Patch clamp analysis of gap junction channel properties. *Gap Junction Channels and Hemichannels*. CRC Press.
- BAI, D., DEL CORSSO, C., SRINIVAS, M. & SPRAY, D. C. 2006. Block of specific gap junction channel subtypes by 2-aminoethoxydiphenyl borate (2-APB). *J. Pharmacol. Exp. Ther.*, 319, 1452-8.
- BAI, D. & WANG, A. H. 2014. Extracellular domains play different roles in gap junction formation and docking compatibility. *Biochem. J.*, 458, 1-10.
- BAI, D., WANG, J., LI, T., CHAN, R., ATALLA, M., CHEN, R. C., KHAZANEH, M. T., AN, R. J. & STATHOPOULOS, P. B. 2021. Differential Domain Distribution of gnomAD- and Disease-Linked Connexin Missense Variants. *Int. J. Mol. Sci.*, 22.
- BAI, D., YUE, B. & AOYAMA, H. 2018. Crucial motifs and residues in the extracellular loops influence the formation and specificity of connexin docking. *Biochim Biophys Acta Biomembr*, 1860, 9-21.
- BARGIELLO, T. A., TANG, Q., OH, S. & KWON, T. 2012. Voltage-dependent conformational changes in connexin channels. *Biochim. Biophys. Acta*, 1818, 1807-22.
- BEYER, E. C., EBIHARA, L. & BERTHOUD, V. M. 2013. Connexin mutants and cataracts. *Front. Pharmacol.*, 4, 43.
- BUKAUSKAS, F. F. & VERSELIS, V. K. 2004. Gap junction channel gating. *Biochim. Biophys. Acta*, 1662, 42-60.
- BUKAUSKAS, F. F. & WEINGART, R. 1994. Voltage-dependent gating of single gap junction channels in an insect cell line. *Biophys. J.*, 67, 613-25.
- CALERA, M. R., TOPLEY, H. L., LIAO, Y., DULING, B. R., PAUL, D. L. & GOODENOUGH, D. A. 2006. Connexin43 is required for production of the aqueous humor in the murine eye. *J. Cell Sci.*, 119, 4510-9.



- COTTRELL, G. T. & BURT, J. M. 2001. Heterotypic gap junction channel formation between heteromeric and homomeric Cx40 and Cx43 connexons. *Am. J. Physiol. Cell Physiol.*, 281, C1559-67.
- DEROSA, A. M., MEŞE, G., LI, L., SELLITTO, C., BRINK, P. R., GONG, X. & WHITE, T. W. 2009. The cataract causing Cx50-S50P mutant inhibits Cx43 and intercellular communication in the lens epithelium. *Exp. Cell Res.*, 315, 1063-75.
- DOBROWOLSKI, R. & WILLECKE, K. 2009. Connexin-caused genetic diseases and corresponding mouse models. *Antioxid Redox Signal*, 11, 283-95.
- DOSHI, D. C., LIMDI, P. K., PAREKH, N. V. & GOHIL, N. R. 2016. Oculodentodigital dysplasia. *Indian J. Ophthalmol.*, 64, 227-30.
- EVANS, W. H., AHMAD, S., DIEZ, J., GEORGE, C. H., KENDALL, J. M. & MARTIN, P. E. 1999. Trafficking pathways leading to the formation of gap junctions. *Novartis Found. Symp.*, 219, 44-54; discussion 54-9.
- EVANS, W. H. & MARTIN, P. E. 2002. Gap junctions: structure and function (Review). *Mol. Membr. Biol.*, 19, 121-36.
- FLORES, J. A., HADDAD, B. G., DOLAN, K. A., MYERS, J. B., YOSHIOKA, C. C., COPPERMAN, J., ZUCKERMAN, D. M. & REICHOW, S. L. 2020. Connexin-46/50 in a dynamic lipid environment resolved by CryoEM at 1.9 Å. *Nat Commun*, 11, 4331.
- FOOTE, C. I., ZHOU, L., ZHU, X. & NICHOLSON, B. J. 1998. The pattern of disulfide linkages in the extracellular loop regions of connexin 32 suggests a model for the docking interface of gap junctions. *J. Cell Biol.*, 140, 1187-97.
- FRASSON, M., CALIXTO, N., CRONEMBERGER, S., DE AGUIAR, R. A., LEÃO, L. L. & DE AGUIAR, M. J. 2004. Oculodentodigital dysplasia: study of ophthalmological and clinical manifestations in three boys with probably autosomal recessive inheritance. *Ophthalmic Genet.*, 25, 227-36.
- GAO, Y. & SPRAY, D. C. 1998. Structural changes in lenses of mice lacking the gap junction protein connexin43. *Invest. Ophthalmol. Vis. Sci.*, 39, 1198-209.
- GOEL, M., PICCIANI, R. G., LEE, R. K. & BHATTACHARYA, S. K. 2010. Aqueous humor dynamics: a review. *Open Ophthalmol J*, 4, 52-9.
- GONG, X., LI, E., KLIER, G., HUANG, Q., WU, Y., LEI, H., KUMAR, N. M., HORWITZ, J. & GILULA, N. B. 1997. Disruption of alpha3 connexin gene leads to proteolysis and cataractogenesis in mice. *Cell*, 91, 833-43.
- GOODENOUGH, D. A. & PAUL, D. L. 2009. Gap junctions. *Cold Spring Harb. Perspect. Biol.*, 1, a002576.

- JIANG, J. X. & GOODENOUGH, D. A. 1996. Heteromeric connexons in lens gap junction channels. *Proc. Natl. Acad. Sci. U. S. A.*, 93, 1287-91.
- KRONENGOLD, J., SRINIVAS, M. & VERSELIS, V. K. 2012. The N-terminal half of the connexin protein contains the core elements of the pore and voltage gates. *J. Membr. Biol.*, 245, 453-63.
- LODDENKEMPER, T., GROTE, K., EVERS, S., OELERICH, M. & STÖGBAUER, F. 2002. Neurological manifestations of the oculodentodigital dysplasia syndrome. *J. Neurol.*, 249, 584-95.
- MAEDA, S., NAKAGAWA, S., SUGA, M., YAMASHITA, E., OSHIMA, A., FUJIYOSHI, Y. & TSUKIHARA, T. 2009. Structure of the connexin 26 gap junction channel at 3.5 Å resolution. *Nature*, 458, 597-602.
- MATHIAS, R. T., KISTLER, J. & DONALDSON, P. 2007. The lens circulation. *J. Membr. Biol.*, 216, 1-16.
- MATHIAS, R. T., WHITE, T. W. & GONG, X. 2010. Lens gap junctions in growth, differentiation, and homeostasis. *Physiol. Rev.*, 90, 179-206.
- MORENO, A. P., CHANSON, M., ELENES, S., ANUMONWO, J., SCERRI, I., GU, H., TAFFET, S. M. & DELMAR, M. 2002. Role of the carboxyl terminal of connexin43 in transjunctional fast voltage gating. *Circ. Res.*, 90, 450-7.
- MUSA, F. U., RATAJCZAK, P., SAHU, J., PENTLICKY, S., FRYER, A., RICHARD, G. & WILLOUGHBY, C. E. 2009. Ocular manifestations in oculodentodigital dysplasia resulting from a heterozygous missense mutation (L113P) in GJA1 (connexin 43). *Eye*, 23, 549-555.
- MUSA, H., FENN, E., CRYE, M., GEMEL, J., BEYER, E. C. & VEENSTRA, R. D. 2004. Amino terminal glutamate residues confer spermine sensitivity and affect voltage gating and channel conductance of rat connexin40 gap junctions. *J. Physiol.*, 557, 863-78.
- MYERS, J. B., HADDAD, B. G., O'NEILL, S. E., CHOREV, D. S., YOSHIOKA, C. C., ROBINSON, C. V., ZUCKERMAN, D. M. & REICHOW, S. L. 2018. Structure of native lens connexin 46/50 intercellular channels by cryo-EM. *Nature*, 564, 372-377.
- NIELSEN, M. S., AXELSEN, L. N., SORGEN, P. L., VERMA, V., DELMAR, M. & HOLSTEIN-RATHLOU, N. H. 2012. Gap junctions. *Compr Physiol*, 2, 1981-2035.
- OH, S., ABRAMS, C. K., VERSELIS, V. K. & BARGIELLO, T. A. 2000. Stoichiometry of transjunctional voltage-gating polarity reversal by a negative charge substitution in the amino terminus of a connexin32 chimera. *J. Gen. Physiol.*, 116, 13-31.

- OH, S. & BARGIELLO, T. A. 2015. Voltage regulation of connexin channel conductance. *Yonsei Med. J.*, 56, 1-15.
- PERACCHIA, C. & PERACCHIA, L. L. 2005. Inversion of both gating polarity and CO<sub>2</sub> sensitivity of voltage gating with D3N mutation of Cx50. *Am. J. Physiol. Cell Physiol.*, 288, C1381-9.
- PURNICK, P. E., OH, S., ABRAMS, C. K., VERSELIS, V. K. & BARGIELLO, T. A. 2000. Reversal of the gating polarity of gap junctions by negative charge substitutions in the N-terminus of connexin 32. *Biophys. J.*, 79, 2403-15.
- RAO, G. N., KHANNA, R. & PAYAL, A. 2011. The global burden of cataract. *Curr. Opin. Ophthalmol.*, 22, 4-9.
- REAUME, A. G., DE SOUSA, P. A., KULKARNI, S., LANGILLE, B. L., ZHU, D., DAVIES, T. C., JUNEJA, S. C., KIDDER, G. M. & ROSSANT, J. 1995. Cardiac malformation in neonatal mice lacking connexin43. *Science*, 267, 1831-4.
- RONG, P., WANG, X., NIESMAN, I., WU, Y., BENEDETTI, L. E., DUNIA, I., LEVY, E. & GONG, X. 2002. Disruption of Gja8 (alpha8 connexin) in mice leads to microphthalmia associated with retardation of lens growth and lens fiber maturation. *Development*, 129, 167-74.
- SANTOS-MIRANDA, A., CHEN, H., CHEN, R. C., ODOKO-ISHIMOTO, M., AOYAMA, H. & BAI, D. 2020. The amino terminal domain plays an important role in transjunctional voltage-dependent gating kinetics of Cx45 gap junctions. *J. Mol. Cell. Cardiol.*, 143, 71-84.
- SELLITTO, C., LI, L. & WHITE, T. 2004. Connexin50 Is Essential for Normal Postnatal Lens Cell Proliferation. *Invest. Ophthalmol. Vis. Sci.*, 45, 3196-202.
- SHIELS, A. & HEJTMANCIK, J. F. 2013. Genetics of human cataract. *Clin. Genet.*, 84, 120-7.
- SIMON, A. M. & GOODENOUGH, D. A. 1998. Diverse functions of vertebrate gap junctions. *Trends Cell Biol.*, 8, 477-83.
- SÖHL, G., MAXEINER, S. & WILLECKE, K. 2005. Expression and functions of neuronal gap junctions. *Nat. Rev. Neurosci.*, 6, 191-200.
- SÖHL, G. & WILLECKE, K. 2004. Gap junctions and the connexin protein family. *Cardiovasc. Res.*, 62, 228-32.
- SPRAY, D. C., HARRIS, A. L. & BENNETT, M. V. 1981. Equilibrium properties of a voltage-dependent junctional conductance. *J. Gen. Physiol.*, 77, 77-93.
- SRINIVAS, M., ROZENTAL, R., KOJIMA, T., DERMIETZEL, R., MEHLER, M., CONDORELLI, D. F., KESSLER, J. A. & SPRAY, D. C. 1999. Functional

- properties of channels formed by the neuronal gap junction protein connexin36. *J. Neurosci.*, 19, 9848-55.
- TEJADA, M. G., SUDHAKAR, S., KIM, N. K., AOYAMA, H., SHILTON, B. H. & BAI, D. 2018. Variants with increased negative electrostatic potential in the Cx50 gap junction pore increased unitary channel conductance and magnesium modulation. *Biochem. J.*, 475, 3315-3330.
- TEUBNER, B., DEGEN, J., SÖHL, G., GÜLDENAGEL, M., BUKAUSKAS, F. F., TREXLER, E. B., VERSELIS, V. K., DE ZEEUW, C. I., LEE, C. G., KOZAK, C. A., PETRASCH-PARWEZ, E., DERMIETZEL, R. & WILLECKE, K. 2000. Functional expression of the murine connexin 36 gene coding for a neuron-specific gap junctional protein. *J. Membr. Biol.*, 176, 249-62.
- TONG, J.-J. & EBIHARA, L. 2006. Structural Determinants for the Differences in Voltage Gating of Chicken Cx56 and Cx45.6 Gap-Junctional Hemichannels. *Biophys. J.*, 91, 2142-2154.
- TONG, X., AOYAMA, H., TSUKIHARA, T. & BAI, D. 2014. Charge at the 46th residue of connexin 50 is crucial for the gap-junctional unitary conductance and transjunctional voltage-dependent gating. *J. Physiol.*, 592, 5187-202.
- VALIUNAS, V. 2002. Biophysical properties of connexin-45 gap junction hemichannels studied in vertebrate cells. *J. Gen. Physiol.*, 119, 147-64.
- VEENSTRA, R. D., WANG, H. Z., BEYER, E. C., RAMANAN, S. V. & BRINK, P. R. 1994. Connexin37 forms high conductance gap junction channels with subconductance state activity and selective dye and ionic permeabilities. *Biophys. J.*, 66, 1915-28.
- VERSELIS, V. K., GINTER, C. S. & BARGIELLO, T. A. 1994. Opposite voltage gating polarities of two closely related connexins. *Nature*, 368, 348-51.
- VINKEN, M. 2015. Introduction: connexins, pannexins and their channels as gatekeepers of organ physiology. *Cell. Mol. Life Sci.*, 72, 2775-8.
- VINKEN, M., VANHAECKE, T. & ROGIERS, V. 2003. [The role of intercellular communication via "gap junctions" in disease]. *Ned. Tijdschr. Geneesk.*, 147, 2463-6.
- WHITE, T. W. 2002. Unique and redundant connexin contributions to lens development. *Science*, 295, 319-20.
- WHITE, T. W., BRUZZONE, R., WOLFRAM, S., PAUL, D. L. & GOODENOUGH, D. A. 1994. Selective interactions among the multiple connexin proteins expressed in the vertebrate lens: the second extracellular domain is a determinant of compatibility between connexins. *J. Cell Biol.*, 125, 879-92.

- WHITE, T. W., GOODENOUGH, D. A. & PAUL, D. L. 1998. Targeted ablation of connexin50 in mice results in microphthalmia and zonular pulverulent cataracts. *J. Cell Biol.*, 143, 815-25.
- WHITE, T. W., SELBITTO, C., PAUL, D. L. & GOODENOUGH, D. A. 2001. Prenatal lens development in connexin43 and connexin50 double knockout mice. *Invest. Ophthalmol. Vis. Sci.*, 42, 2916-23.
- WILLECKE, K., EIBERGER, J., DEGEN, J., ECKARDT, D., ROMUALDI, A., GÜLDENAGEL, M., DEUTSCH, U. & SÖHL, G. 2002. Structural and functional diversity of connexin genes in the mouse and human genome. *Biol. Chem.*, 383, 725-37.
- XIN, L. & BAI, D. 2013. Functional roles of the amino terminal domain in determining biophysical properties of Cx50 gap junction channels. *Front. Physiol.*, 4, 373.
- XIN, L., GONG, X. Q. & BAI, D. 2010. The role of amino terminus of mouse Cx50 in determining transjunctional voltage-dependent gating and unitary conductance. *Biophys. J.*, 99, 2077-86.
- XIN, L., NAKAGAWA, S., TSUKIHARA, T. & BAI, D. 2012. Aspartic acid residue D3 critically determines Cx50 gap junction channel transjunctional voltage-dependent gating and unitary conductance. *Biophys. J.*, 102, 1022-31.
- YUE, B., HADDAD, B. G., KHAN, U., CHEN, H., ATALLA, M., ZHANG, Z., ZUCKERMAN, D. M., REICHOW, S. L. & BAI, D. 2021. Connexin 46 and connexin 50 gap junction channel properties are shaped by structural and dynamic features of their N-terminal domains. *J. Physiol.*, 599, 3313-3335.
- ZOIDL, G. & DERMIETZEL, R. 2010. Gap junctions in inherited human disease. *Pflugers Arch.*, 460, 451-66.

## 2 Manuscript

### 2.1 Abstract

Gap junctions (GJs) are intercellular channels composed of 12 connexin subunits that promote chemical and electrical coupling between adjacent cells. The eye lens expresses three types of connexins: Cx43, Cx46, and Cx50. Recently, the GJs of Cx46 and Cx50 structures were resolved by Cryo-EM at 1.9 Å resolution opening the door for structure-function studies. The structures show the amino terminal (NT) domain as an amphipathic  $\alpha$ -helix where hydrophobic residues interact with hydrophobic residues on transmembrane (M1/2) domains of the same or neighboring subunit to anchor the NT in an open state conformation. To test these novel structural models experimentally, we generated four pairs of variants on the 10<sup>th</sup>, 13<sup>th</sup>, 14<sup>th</sup>, and 15<sup>th</sup> positions of Cx46 and Cx50 and assessed their ability to form functional GJs, their  $V_j$ -gating properties, and single channel conductance in connexin-deficient N2A cell pairs via dual whole-cell voltage clamp technique. Our data revealed an important role of the two hydrophobic residues (L10 and A14) in Cx46 GJs as A14V variant showed reduced coupling conductance ( $G_j$ ) partially due to a decreased  $\gamma_j$  whereas L10I affected the  $V_j$ -gating. Interestingly, mutation with an increased side chain size on M2 of Cx50, S89T, which is predicted to interact with V14 of the NT, completely impairs GJ function. Our results also revealed an important role of the 13<sup>th</sup> residues of both Cx46 and Cx50 as N13E and E13N variant GJs showed reduction in coupling% (N13E), or in both cases the  $G_j$  and  $\gamma_j$ . Cx50 N15Q showed reduction in  $G_j$  and  $\gamma_j$  as well. In contrast, no significant changes in  $V_j$ -gating or  $\gamma_j$  were observed in Cx46 Q15N, Cx50 I10L and V14A. Our results provide novel insights on how NT domain play a role in  $V_j$ -gating and control rate of ion permeation and contribute to the understanding of structure-function relationship for these important lens GJs.

## 2.2 Introduction

Gap junctions (GJs) promote direct intercellular communications by permitting the passage of not only ions ( $\text{Na}^+$ ,  $\text{K}^+$ ,  $\text{Ca}^{2+}$ ,  $\text{Cl}^-$ ), but also metabolic (glucose, amino acid) and signaling molecules (cAMP, cGMP, inositol trisphosphate (IP3)) that are under 1 kDa in size, thereby optimizing tissue homeostasis and normal organ function (Goodenough et al., 1996, Meşe et al., 2007, Goldberg et al., 2004). Consequently, dysfunction in GJs have been shown to play a role in a variety of pathological conditions such as, stroke, heart failure, cardiac arrhythmia, cataract, deafness, skin disorders and several types of cancers (Lo, 2000, Gerido and White, 2004, Orellana et al., 2014, Sinyuk et al., 2018). GJs are composed of different integral protein subunits, named connexins. Six connexins oligomerize into a cylindrical channel shape across the plasma membrane and form a connexon or hemichannel. Two hemichannels dock together to form one gap junction channel (Goodenough et al., 1996, Söhl et al., 2005). There are 21 identified connexin genes in humans which express connexin polypeptides that vary in protein size and amino acid sequence yet share similar structural topology. All connexins consist of four transmembrane domains (M1-M4) connected by two extracellular loops (E1 and E2) and one cytoplasmic loop (CL), as well as the cytosolic amino and carboxyl termini (NT and CT, respectively) (Goodenough and Paul, 2009). Transmembrane domains, extracellular loops, and the NT domain are highly conserved among different connexins (Abascal and Zardoya, 2013). Different tissues form different gap junction channels that serve specialized functions to satisfy their homeostasis (Goodenough and Paul, 2009).

Functional characterization of GJs formed by different connexins showed diverse channel properties, including a wide range of ion permeation rates, distinct selectivity to different ions and small molecules, and different gating control by divalent cations (e.g.  $\text{Ca}^{2+}$  and  $\text{Mg}^{2+}$ ), pH levels, and transjunctional voltage ( $V_j$ ). Transjunctional voltage-dependent gating (also known as  $V_j$ -gating) is a common property of all GJs. GJs formed by different connexins displayed distinct level of  $V_j$ -gating extent, half deactivation voltage, gating sensitivity (also known as gating charge), and/or gating kinetics (Bukauskas and Verselis, 2004, González et al., 2007). The rate of ion permeation (measured by single channel conductance or  $\gamma_j$ ) of GJs formed by different connexins range from a few pico-

Siemens (pS) to hundreds of pS (Veenstra et al., 1994, Moreno et al., 2002, Pellegrini-Calace et al., 2009, Teubner et al., 2000). The molecular and structural mechanisms for controlling GJ channel gating properties and ion permeation are not fully clear.

Many electrophysiological studies provided compelling evidence that the amino-terminal domain (NT) and the residues within the NT of Cx26, Cx32, Cx40, Cx46, and Cx50 are critical for their  $V_j$ -gating polarity, gating extent, gating sensitivity and kinetics, channel open stability, and single channel conductance ( $\gamma_j$ ) (Purnick et al., 2000, Myers et al., 2018, Xin and Bai, 2013, Tong and Ebihara, 2006, Peracchia and Peracchia, 2005, Musa et al., 2004, Verselis et al., 1994, Xin et al., 2010, Xin et al., 2012, Kronengold et al., 2012, Srinivas et al., 1999, Tong et al., 2014). Most of these studies are more focused on the charge changes in the NT region or the entire NT domain and support a GJ gating model where the NT domain exists in the pore and is capable of sensing the  $V_j$ , also contributing, at least partially, to the electrostatic properties of the pore for ion permeation. Other residues, including hydrophobic residues, have not been clearly defined with respect to their role in  $V_j$ -gating and ion permeation.

The first high resolution (3.5 Å) crystal structure resolved was of human Cx26 GJ where the NT domain folded into the channel and lined the vestibule part of GJ pore. Collectively, six NT domains of each hemichannel form a funnel structure comprising the narrowest part of the GJ (Maeda et al., 2009, Maeda and Tsukihara, 2011). These structural features of the NT domain make it suitable for sensing voltage differences across the channel and suggest that it forms a constriction site to regulate the rate of ion permeation and selectivity, which could affect both  $V_j$ -gating and single channel properties. Molecular simulation studies based on this structure model revealed that the NT domain of Cx26 is highly dynamic and the structure of the NT could be rapidly disordered without chemical modification or freezing (Kwon et al., 2011, Luo et al., 2016, Villanelo et al., 2017). Consistent with these studies, a few GJ structure models of Cx26 were unable to resolve the NT domain structure (Bennett et al., 2016, Khan et al., 2020), questioning the structural anchoring mechanism for the NT domain in the GJ pore. More recently, high resolution cryogenic electron microscopy (Cryo-EM) structures of native sheep Cx46 and Cx50 GJs, at 3.4 Å and later 1.9 Å resolutions, were resolved



(Myers et al., 2018, Flores et al., 2020). Most domains in Cx46 and Cx50 show a similar structure as those of Cx26 (Fig. 2-1), including the NT domains in Cx46 and Cx50 GJs, which are positioned in the vestibule to form the narrowest part of the channel. However, this NT domain displayed the largest structural difference from that of Cx26 with very different orientations and local interactions (Fig. 2-1). Specifically, the NT domain adopts an amphipathic  $\alpha$ -helix in which the hydrophobic amino acids are packed against the transmembrane (M1 and M2) domains forming hydrophobic interactions, which stabilize the NT domain in the open conformation of Cx46 and Cx50 GJs while the hydrophilic side is facing into the pore and could play a role in voltage sensing and ion/substrate selectivity (Myers et al., 2018, Flores et al., 2020). Hydrophobic interactions between NT and M1/M2 domains in Cx46 and Cx50 GJ are a novel anchoring mechanism to stabilize the NT domain. In addition, the large difference in Cx46 and Cx50 NT domain compared to Cx26 revealed many different intra- and inter-subunit salt-bridge interactions in this domain. Hydrophobic residues in the NT domains of all connexins are highly conserved (see Fig. 3-2) underlying their critical role in GJ function.

To start testing these novel structural features and their influences on  $V_j$ -gating and ion permeation in the Cx46 and Cx50 connexins, we designed a series of missense variant pairs in the sheep Cx46 and Cx50 NT domain where we switched corresponding residues one by one as shown in Fig. 2-2 and studied the  $V_j$ -gating properties and single channel conductance of these variants with dual patch clamp technique. Our experimental data together with homology modeling in this and our previous study (Yue et al., 2021) demonstrated an important role for hydrophobic interactions between the NT and M2 domains in mediating GJ channel unitary channel conductance of these lens GJs. Our observations possibly extend to other connexin GJs.

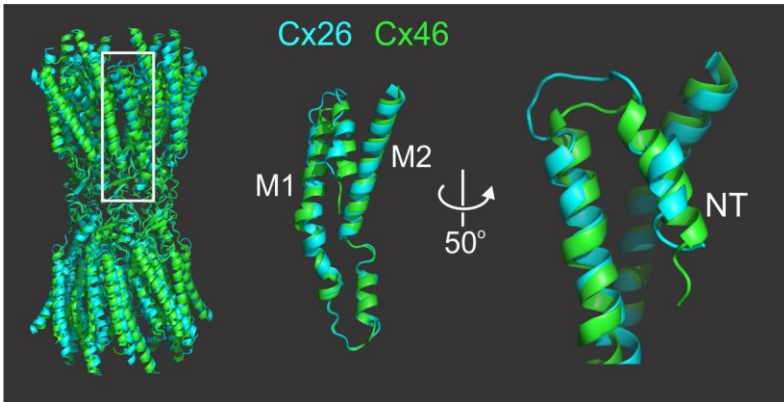


**Figure 2-1:** The NT domains of Cx26 and Cx46 are different in spatial orientations with respect to the transmembrane domains (M1 and M2). GJ structures of Cx26 (cyan) and Cx46 (green) are aligned (left panel). Part of one subunit with NT, M1, E1 and M2 are shown in the middle and right panel to show the different orientations of the NT domains of these GJ models.

## NT domains



**Figure 2-2:** Amino acid sequence alignment of sheep Cx46 and Cx50. Different amino acid residues between the two connexins are indicated by asterisks. Our designed missense variants are listed next to their parental connexin. A grey asterisk on the 9<sup>th</sup> position indicates that both Cx46 N9R and Cx50 R9N were studied by us earlier (Yue et al., 2021).

## 2.3 Materials and Methods

### 2.3.1 Plasmid construction

Complementary DNA (cDNA) for both sheep Cx46 (sCx46, also known as Cx44) and Cx50 (sCx50, also known as Cx49) were synthesized and each of them was inserted into an expression vector, pIRES2-EGFP, with an untagged GFP reporter between the restriction enzyme sites, XhoI and EcoRI (NorClone Biotech Laboratories, London, Ontario), as previously described (Noureldin et al., 2018, Jassim et al., 2016). The sCx46 and sCx50 variants (sCx46-L10I, N13E, A14V, Q15N and sCx50-I10L, E13N, V14A, N15Q, and S89T) were generated by PCR-mediated site-directed mutagenesis using the corresponding untagged wildtype constructs as templates with the appropriate primers. All wildtype and variant constructs were sequenced to confirm the accuracy of the nucleotide sequences. The primers used to generate these point variants are listed below:

sCx46 L10I: forward 5' GC TTC CTG GGG AGA ATC CTA GAG AAC GCC CAG 3'  
and reverse 5' CTG GGC GTT CTC TAG GAT TCT CCC CAG GAA GC 3'

sCx46 N13E: forward 5' GG AGA CTC CTA GAG GAG GCC CAG GAG CAC TCC 3'  
and reverse 5' GGA GTG CTC CTG GGC CTC CTC TAG GAG TCT CC 3'

sCx46 A14V: forward 5' CTC CTA GAG AAC GTG CAG GAG CAC TCC 3' and  
reverse 5' GGA GTG CTC CTG CAC GTT CTC TAG GAG 3'

sCx46 Q15N: forward 5' C CTA GAG AAC GCC AAT GAG CAC TCC ACT G 3' and  
reverse 5' C AGT GGA GTG CTC ATT GGC GTT CTC TAG G 3'

sCx50 I10L: forward 5' GT TTC CTG GGG AAC CTC TTG GAG GAG GTG 3' and  
reverse 5' CAC CTC CTC CAA GAG GTT CCC CAG GAA AC 3'

sCx50 E13N: forward 5' G GGG AAC ATC TTG GAG AAC GTG AAT GAG CAC 3'  
and reverse 5' GTG CTC ATT CAC GTT CTC CAA GAT GTT CCC C 3'

sCx50 V14A: forward 5' C ATC TTG GAG GAG GCC AAT GAG CAC TCC ACG 3'  
and reverse 5' CGT GGA GTG CTC ATT GGC CTC CTC CAA GAT G 3'

sCx50 N15Q: forward 5' C TTG GAG GAG GTG CAG GAG CAC TCC ACG 3' and  
reverse 5' CGT GGA GTG CTC CTG CAC CTC CTC CAA G 3'

sCx50 S89T: forward 5' GTC TCC ACG CCG ACG CTG GTG TAC GTG 3' and  
reverse 5' CAC GTA CAC CAG CGT CGG CGT GGA GAC 3'

### 2.3.2 Cell culture and transient transfections

Connexin-deficient mouse neuroblastoma (N2A) cells were used in these studies (American Type Culture Collection, Manassas, VA, USA). On the day before transfection, N2A cells were passaged in 35 mm dishes with Dulbecco's modified Eagle's medium (DMEM) containing 10% fetal bovine serum (FBS) (Life Technologies Corporation, Grand Island, NY, USA) to attain around 70% confluence after overnight incubation. The subsequent day, the N2A cells were transfected with 1  $\mu$ g of each construct using 2  $\mu$ L of X-tremeGENE HP DNA transfection reagent (Roche Diagnostics GmbH, Indianapolis, IN, USA) in Opti-MEM + GlutaMAX-I medium (Life Technologies Corporation, Grand Island, NY, USA). After 5 h, the medium was changed back to FBS-containing DMEM, and the cells were incubated overnight. On the third day, transfected cells with Cx46 or Cx46 variants were replated onto coverslips for 2 h before transfer to the recording chamber, while N2A cells expressing Cx50 or Cx50 variants were replated for 5 h, each at 50-70% density. Only isolated cell pairs with expression of GFP were selected for dual patch clamp recording.

### 2.3.3 Electrophysiological recordings

Glass coverslips with transfected cells were transferred to a recording chamber on a fluorescent microscope (BX51WI, Olympus) using a 40x water immersion lens and FITC or a dual (red and green emission) filter. The chamber was filled with extracellular solution (ECS) [pH 7.4, osmolarity 310-320 mOsm] at room temperature. The ECS contained (in mM): 135 NaCl, 2 CsCl, 2 CaCl<sub>2</sub>, 1 MgCl<sub>2</sub>, 1 BaCl<sub>2</sub>, 10 HEPES, 5 KCl, 5 D-(+)-glucose, 2 sodium pyruvate. The dual whole-cell voltage clamp technique was then used to characterize the GJs in isolated reporter GFP-positive cell pairs. Patching glass micropipettes were pulled using a micropipette puller (PC-10, Narishige International USA Inc., Amityville, NY, USA). These micropipettes were subsequently filled with intracellular solution (ICS) containing (in mM): 130 CsCl, 10 EGTA, 0.5 CaCl<sub>2</sub>, 5 Na<sub>2</sub>ATP, 10 HEPES [pH 7.2, osmolarity 290-300 mOsm]. One of the cells was voltage clamped at 0 mV (junctional current recording cell), while a series of voltage pulses

ranging from  $\pm 20$  to  $\pm 100$  mV (pulsing cell) was administered to the other cell to establish transjunctional voltage ( $V_j$ ). If functional GJ channels existed between the cell pairs, a transjunctional current ( $I_j$ ) was measured at the recording cell via a patch clamp amplifier (MultiClamp 700A, Molecular Devices, Sunnyvale, CA, USA) with a low-pass filter (cut-off frequency 1 kHz) and digitized at a 10 kHz sampling rate via an ADDA converter (Digidata 1322A; Molecular Devices, Sunnyvale, CA, USA).

### 2.3.4 Transjunctional voltage dependent gating

A voltage-step protocol ( $\pm 20$  to  $\pm 100$  mV with 20 mV increment) was applied on the “pulsing cell” of the cell pair expressing the construct of interest to establish transjunctional voltage ( $V_j$ ). Transjunctional current ( $I_j$ ) was then obtained in the recording cell.  $V_j$  dependent gating ( $V_j$ -gating) reflects the  $I_j$  amplitude decline with time at high  $V_j$  ( $\pm 40$ -100 mV). Coupling conductance ( $G_j$ ) can be calculated via the equation ( $G_j = I_j/V_j$ ). Only cell pairs with  $G_j$  lower than 9 nS were chosen to study the  $V_j$ -gating to minimize the errors of series resistance (Musa et al., 2004, Bai and Cameron, 2016, Moreno et al., 1994, Wilders and Jongsma, 1992). The peak amplitude of junctional current ( $I_{\text{peak}}$ ) was measured at the beginning of the trace, while the steady-state amplitude ( $I_{\text{ss}}$ ) was measured by taking the average junctional current of the last 500 ms of each trace. The steady state  $G_j$  is normalized to the peak  $G_j$  to obtain a normalized steady-state junctional conductance ( $G_{j,\text{ss}}$ ) which can be plotted with the entire tested  $V_j$  range. This  $G_{j,\text{ss}} - V_j$  relationship can be described by a two-state Boltzmann equation:

$$G_{j,\text{ss}} = \frac{G_{\text{max}} - G_{\text{min}}}{1 + \exp [A(V_j - V_0)]} + G_{\text{min}}$$

$V_0$  is the voltage at which the conductance is reduced by half [ $(G_{\text{max}} - G_{\text{min}})/2$ ],  $G_{\text{max}}$  is the maximum normalized conductance,  $G_{\text{min}}$  is the normalized voltage-insensitive residual conductance, and parameter  $A$  is the slope of the fitted curve which reflects the  $V_j$  sensitivity (Bukauskas and Weingart, 1994, González et al., 2007).

### 2.3.5 Single channel analysis

Unitary channel currents ( $i_{js}$ ) can be identified in poorly coupled cell pairs with 1 – 3 GJ channels. The recorded currents were filtered using low pass Gaussian filter (200 Hz) in Clampfit10.3 (Molecular Devices, Sunnyvale, CA, USA). All-point histograms were used to determine baseline and open state amplitude for each current after fitting these histograms with Gaussian functions. Average  $i_{js}$  at each  $V_j$  (regardless of  $V_j$  polarity) of different cell pairs were used to generate the  $i_j$ - $V_j$  plot. Single channel conductance ( $\gamma_j$ ) was estimated by measuring the slope of  $i_j$ - $V_j$  fit using linear regression.

### 2.3.6 Homology structure modeling

Homology structure models of missense variants were generated based on their respective template using Modeller (version 9.17, Andrej Sali Lab, San Francisco, CA, USA). For example, each of the Cx46 variants was based on the Cx46 GJ cryogenic electron microscopy-derived structure (7JKC) and the Cx50 variants were based on Cx50 GJ cryogenic electron microscopy-derived structure (7JJP) (Flores et al., 2020). PyMOL (version 2.4.1) was used for the cartoon representations of the backbone structure with variants of interests using stick/sphere view as needed.

### 2.3.7 Statistical Analysis

Data are presented as mean  $\pm$  standard deviation (SD). Unpaired Two-Samples T-test or Mann–Whitney U test were used to compare coupling percentage,  $G_j$ , and  $\gamma_j$  of each variant to its corresponding wildtype as appropriate. Statistical significance is indicated with asterisks (\* $p < 0.05$ , \*\* $p < 0.01$ , \*\*\* $p < 0.001$ ). Data were analyzed and plotted using GraphPad Prism version 9.31 for Windows (GraphPad Software, La Jolla California USA).

## 2.4 Results

### 2.4.1 Homotypic Cx46 and Cx50 variants form functional GJ channels.

To investigate the effects of switching individual NT residues between the Cx46 and Cx50 on their ability to form functional GJs, we generated 4 pairs of point variants where a single residue at 10<sup>th</sup>, 13<sup>th</sup>, 14<sup>th</sup>, or 15<sup>th</sup> positions of the NT domain was switched with the equivalent residue between Cx46 and Cx50 (see Fig. 2-3). These point variants are L10I, N13E, A14V or Q15N in Cx46, and I10L, E13N, V14A or N15Q in Cx50. All of them as well as wildtype Cx46 and Cx50 are inserted in an expression vector with an untagged GFP as reporter, for example Cx46 L10I-IRES-GFP. Transient transfection of each of these constructs into N2A cells resulted in successful expression of GFP. Isolated GFP-positive cell pairs were selected for dual patch clamp to check their coupling status. GJ coupled cell pairs were readily identifiable with successful recording of junctional currents ( $I_{js}$ ) in response to a 20 mV  $V_j$  pulse (Fig. 2-3A). In cell pairs expressing wildtype, Cx46 showed an average coupling percentage (or coupling%) of  $59 \pm 20\%$  (N=12 transfections) and for Cx50 the coupling% was  $64 \pm 27\%$  (N= 12 transfections) (Fig. 2-3B). Recording was also made on cell pairs expressing each of our designed variants and the coupling% of all the variants were not statistically different from their corresponding wildtype connexin with the exception of Cx46 N13E where a reduced coupling% ( $31 \pm 21\%$ , N= 6 transfections, \* $p = 0.016$ ) was observed, indicating that all of these variants, but N13E, were able to form functional GJs similar to their wildtype connexins.

Next, coupling conductance ( $G_j$ ) was calculated from coupled cell pairs expressing one of the variants or wildtype connexin (Fig.2-3C). The average  $G_{js}$  of Cx46 L10I ( $2.38 \pm 6.01$  nS,  $n = 18$ ) and Q15N ( $2.98 \pm 2.97$  nS,  $n = 12$ ) were similar to that of wildtype Cx46 ( $4.85 \pm 8.09$  nS,  $n = 29$ ,  $p > 0.05$  for each of these two variants). In contrast, the  $G_{js}$  of Cx46 N13E ( $0.39 \pm 0.38$  nS,  $n = 9$ , \*\*\* $p < 0.001$ ) and A14V ( $0.77 \pm 0.60$  nS,  $n = 18$ , \*\* $p = 0.007$ ) were significantly reduced compared to wildtype Cx46. The  $G_{js}$  of the Cx50 I10L ( $1.70 \pm 2.20$  nS,  $n = 9$ ) and V14A ( $2.03 \pm 1.94$  nS,  $n = 10$ ) variants were similar to wildtype Cx50 ( $2.84 \pm 3.07$  nS,  $n = 27$ ,  $p > 0.05$  for each of these two variants), whereas

the  $G_{js}$  of Cx50 E13N ( $2.07 \pm 5.24$  nS,  $n = 23$ ,  $**p = 0.009$ ) and N15Q ( $1.28 \pm 1.48$  nS,  $n = 17$ ,  $*p = 0.021$ ) were significantly reduced compared to wildtype Cx50.



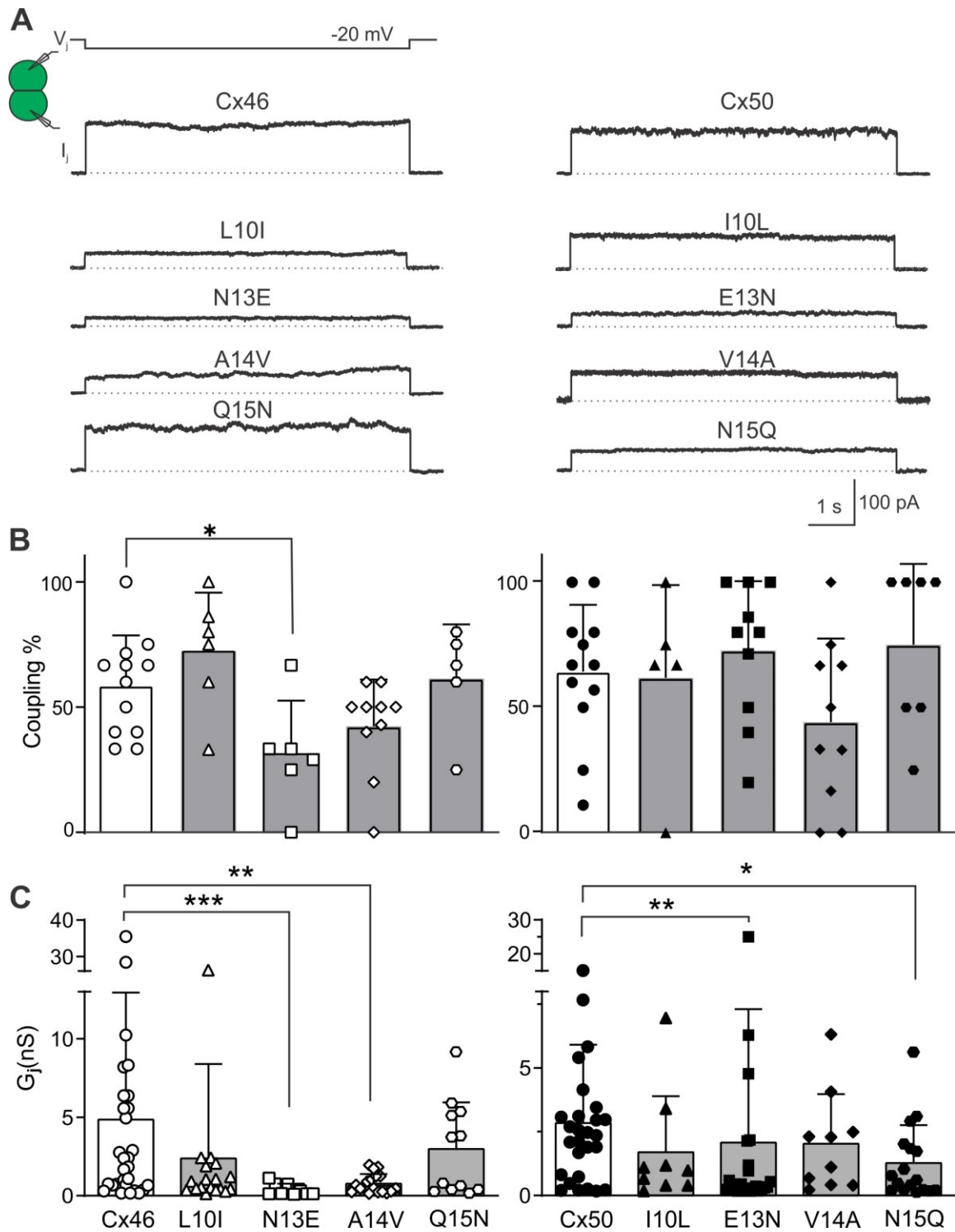


**Figure 2-3:** Coupling percentage and conductance ( $G_j$ ) of N2A cell pairs expressing homotypic wildtype Cx46, Cx50, and their variants on 10<sup>th</sup>, 13<sup>th</sup>, 14<sup>th</sup>, and 15<sup>th</sup> positions in the NT domain as indicated. (A) A typical transjunctional current ( $I_j$ ) is shown for

N2A cell pairs expressing one of the designed missense variants or wildtype as indicated. Expression of each of these variants was successfully leading to GJ coupling with  $I_{js}$  recorded in response to a  $-20$  mV  $V_j$  pulse delivered to the other cell of the pair as shown. (B) Bar graphs illustrate mean coupling% + SD for each of the Cx46 (B1) or Cx50 variants (B2). Each data point represents coupling% for one transfection and 3-10 successful recordings were included to calculate coupling% for each transfection. Only Cx46 N13E variant showed a reduced coupling% than that of Cx46 (\* $p = 0.016$ ). Unpaired Two-Samples T-test or Mann–Whitney U test were used to compare each variant to corresponding wildtype as appropriate. (C) Bar graph shows averaged coupling conductance ( $G_j$ ) of coupled N2A cell pairs expressing each of the variants as indicated. The error bars represent SD. Cell pairs expressing Cx46 N13E and A14V showed significantly lower  $G_j$  compared to Cx46, while Cx50 E13N and N15Q displayed a significantly reduced  $G_j$  compared to Cx50. Mann-Whitney test was used to compare each variant's  $G_j$  to the corresponding wildtype as appropriate. Empty vector-transfected (IRES-GFP) N2A cells were used as negative controls for these experiments and none of them showed any  $I_{js}$ .

#### 2.4.2 $V_j$ -gating properties of the homotypic GJs formed by Cx46 or Cx50 NT variants.

To investigate transjunctional voltage-dependent gating ( $V_j$ -gating) of cell pairs expressing one of the Cx46 or Cx50 NT variants, dual whole-cell voltage clamp technique was used with one of the cells stepping to a series of voltage pulses ( $\pm 20$  to  $\pm 100$  mV in 20 mV increments) and recording junctional current ( $I_{js}$ ) from the other cell. The  $I_{js}$  from cell pairs expressing either Cx46 or Cx50 showed  $V_j$ -dependent mirror-symmetrical deactivation in response to those absolute  $V_{js} \geq 40$  mV (Fig. 2-4A). The steady state conductance near the end of each  $I_j$  is normalized to the peak conductance to obtain the normalized steady state conductance ( $G_{j,ss}$ ), which was plotted as a function of tested  $V_{js}$  ( $G_{j,ss} - V_j$  plot as show in Fig. 2-4B). Data in  $G_{j,ss} - V_j$  plots for both Cx46 and Cx50 GJ could be fitted well with Boltzmann equations on each  $V_j$  polarity to obtain the following parameters:  $G_{max}$ , the maximum normalized conductance;  $G_{min}$ , the minimum normalized conductance; half deactivation voltage  $V_0$  (at which the normalized

conductance =  $(G_{\max} + G_{\min})/2$ ); and the slope  $A$ , which describes the  $V_j$ -gating sensitivity.  $G_{j,ss}$  plot revealed near mirror- symmetrical  $G_{j,ss}$  reduction for both polarities (Fig. 2-4B). The Boltzmann equation fit both datasets well, with the extracted  $G_{\min}$ ,  $G_{\max}$ ,  $V_0$  and  $A$  parameters not significantly different between the wildtype Cx46 and Cx50 expressing cell pairs.

Next,  $I_{js}$  were recorded followed by the assessment of  $G_{j,ss} - V_j$  plots for each of the Cx46 NT variants: L10I, N13E, A14V, and Q15N. Cell pairs expressing the N13E, A14V or Q15N variants showed near mirror-symmetrical deactivation of  $I_{js}$  for both  $V_j$  polarities, whereas cell pairs expressing L10I showed  $I_j$  deactivation on the +  $V_j$  polarity but little  $I_j$  deactivation on the - $V_j$  polarity (Fig. 2-5A). All variant-derived  $G_{j,ss} - V_j$  plots could be described well with Boltzmann equations, except the - $V_j$  for L10I, where no consistent  $V_j$ -gating was observed (Fig. 2-5B). The Boltzmann fitting parameters on GJs formed by the Cx46 NT variants were not significantly different from those of wildtype Cx46 GJ (Table 2-1).

Similarly,  $I_{js}$  were recorded in response to the  $V_j$  protocol in cell pairs expressing each of the Cx50 NT variants: I10L, E13N, V14A, or N15Q. The GJs formed from each of these variants showed nearly mirror symmetrical  $I_{js}$  which deactivated to a similar level at  $V_{js} \geq 40$  mV. Each of the Cx50 NT variant-derived  $G_{j,ss} - V_j$  plots was fitted well with Boltzmann equation for each  $V_j$  polarity (Fig. 2-6B). The Boltzmann fitting parameters of these Cx50 NT variants were not significantly different than those of wildtype Cx50 at each corresponding  $V_j$  polarity (Table 2-2).

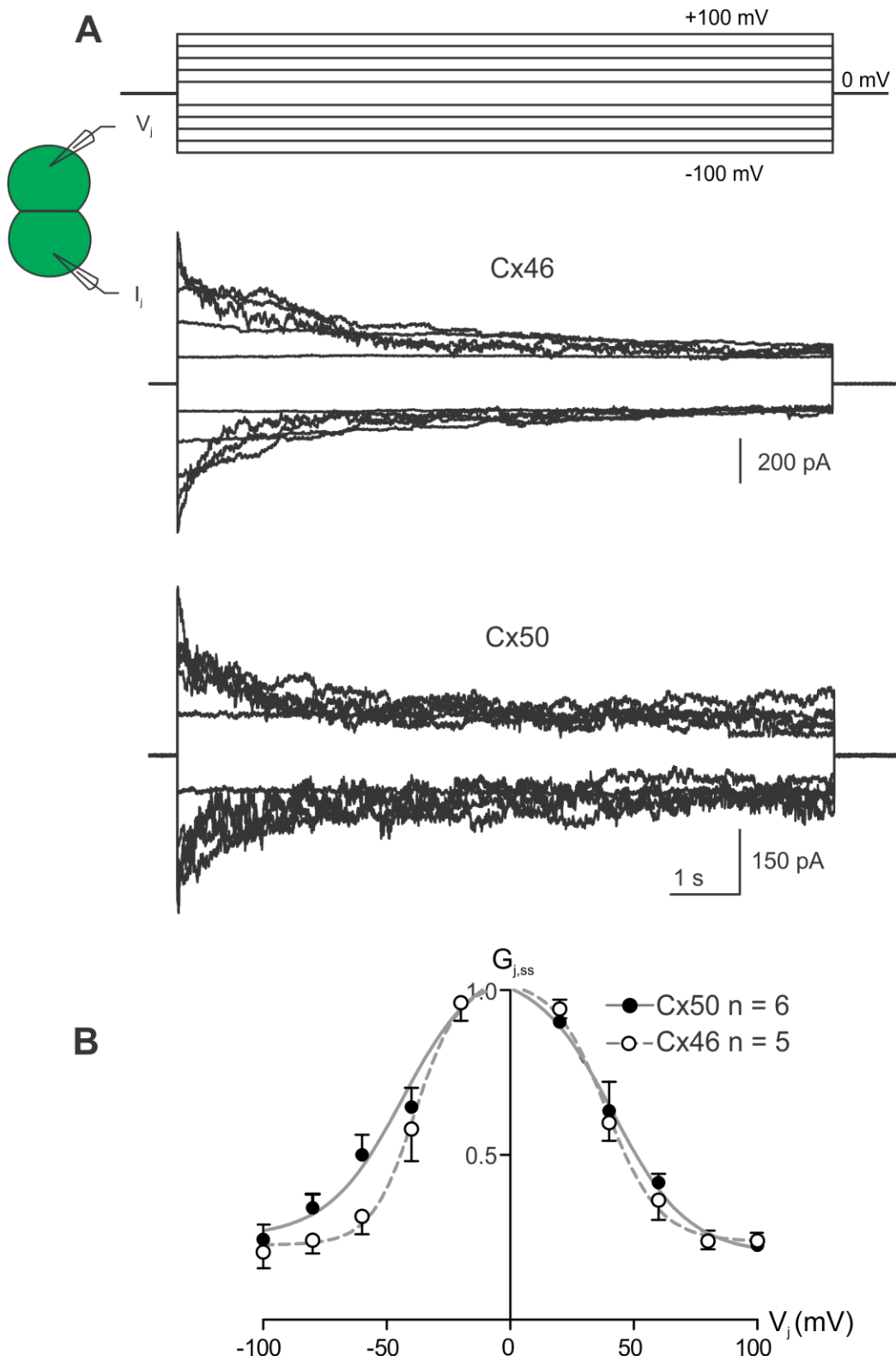


**Figure 2-4:**  $V_j$ -gating of homotypic Cx46, Cx50 gap junction channels. (A) Superimposed junctional currents ( $I_j$ s) from cell pairs expressing wildtype Cx46 or Cx50

in response to a series of voltage pulses ( $V_j$ s) ranging from  $\pm 20$  to  $\pm 100$  mV in 20 mV increments as shown at the top. (B) Normalized steady state junctional conductance ( $G_{j,ss}$ ) was plotted against tested  $V_j$  range for Cx46 (open circles) and Cx50 (solid circles) GJs. Boltzmann equation was used to fit the  $G_{j,ss} - V_j$  plot of Cx46 (smooth dashed black line) and Cx50 (smooth solid black line). Error bars represent SD. Number of cell pairs analyzed are indicated.

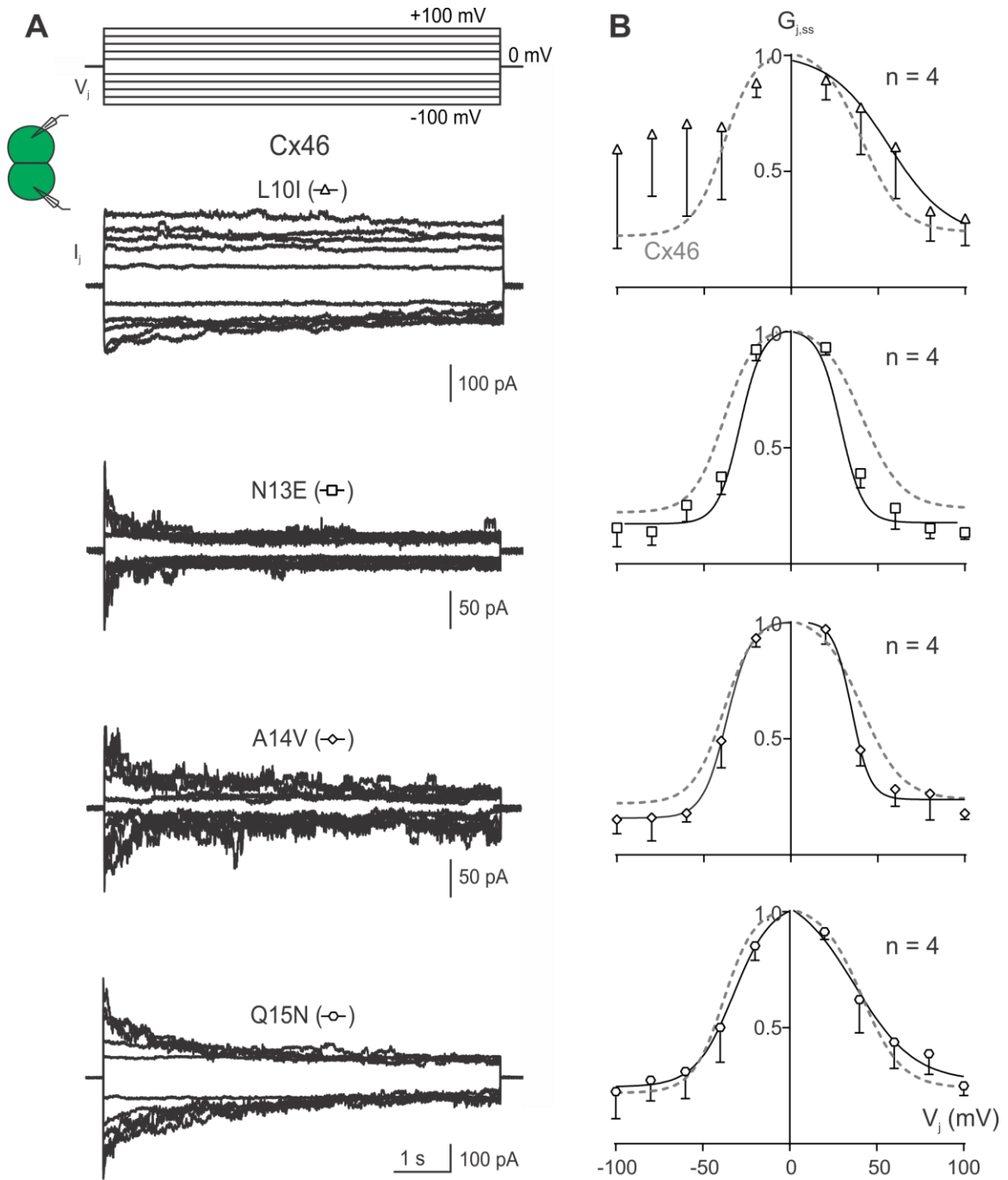


**Figure 2-5:**  $V_j$ -gating properties of GJs formed by Cx46 variants, L10I, N13E, A14V, and Q15N. (A) Superimposed  $I_j$ s from cell pairs expressing L10I, N13E, A14V, and Q15N are illustrated in response to a series of voltage pulses ( $V_j$ s) ranging from  $\pm 20$  to  $\pm 100$  mV in 20 mV increments as shown at the top. (B) Normalized steady state junctional conductance ( $G_{j,ss}$ ) plotted against tested  $V_j$  range for L10I (open triangles),

N13E (open squares), A14V (open diamonds), and Q15N (open hexagons) GJs. The Boltzmann fitted curves (smooth solid black lines) for each of the variants are superimposed with those of wildtype Cx46 (smooth dashed gray line) for easy direct comparison. The number of cell pairs for each variant is indicated on each plot. Error bars represent SD.

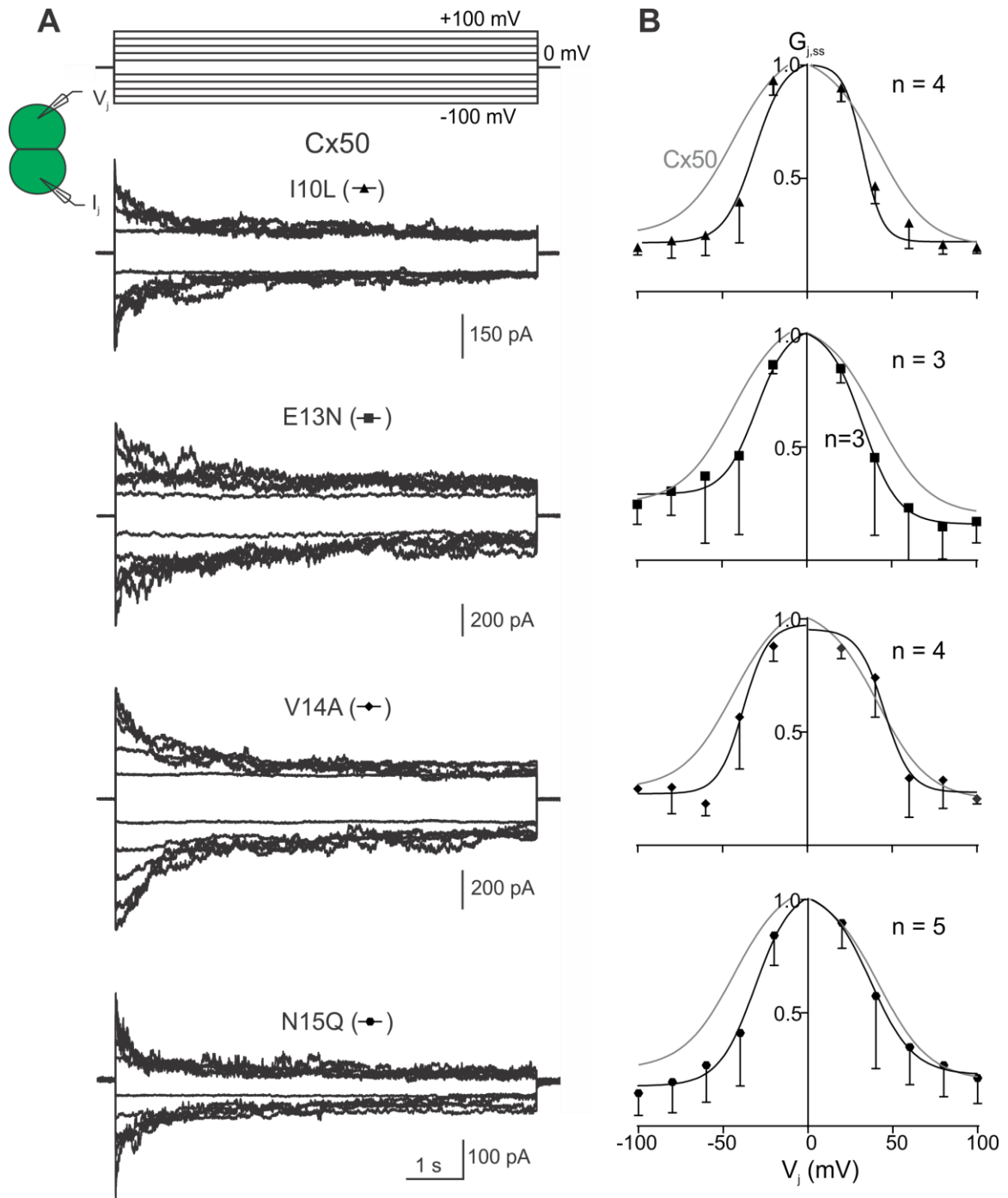


**Figure 2-6:**  $V_j$ -gating properties of the GJs formed by Cx50 variants, I10L, E13N, V14A, or N15Q. (A) Superimposed junctional currents ( $I_j$ ) from cell pairs expressing I10L, E13N, V14A, and N15Q are illustrated in response to a series of voltage pulses ( $V_j$ ) ranging from  $\pm 20$  to  $\pm 100$  mV in 20 mV increments. (B) Normalized steady state junctional conductance ( $G_{j,ss}$ ) plotted against tested  $V_j$  range for I10L (solid triangles),



E13N (solid squares), V14A (solid diamonds), and N15Q (solid hexagons) GJs. The Boltzmann fitted curves (smooth solid black lines) for variants and for wildtype Cx50 (smooth solid gray lines) are superimposed for direct comparison. The number of cell pairs for each variant is indicated on the respective plot. Error bars represent SD.

**Table 2-1:** Boltzmann fitting parameters for the GJs of Cx46 and its variants.

<b>GJs</b>	<b>V<sub>j</sub> polarity</b>	<b>G<sub>max</sub></b>	<b>G<sub>min</sub></b>	<b>V<sub>0</sub></b>	<b>A</b>
Cx46 (n=5)	+	1.03 ± 0.11	0.24 ± 0.07	39.1 ± 5.5	0.09 ± 0.04
	-	1.03 ± 0.13	0.23 ± 0.09	38.6 ± 6.8	0.11 ± 0.09
Cx46 L10I (n=4)	+	1.01 ± 0.08	0.22 ± 0.30	56.1 ± 17.8	0.06 ± 0.06
	-	N/A	N/A	N/A	N/A
Cx46 N13E (n=4)	+	1.01 ± 0.06	0.17 ± 0.04	33.6 ± 3.6	0.16 ± 0.06
	-	1.01 ± 0.08	0.17 ± 0.04	32.9 ± 1.8	0.15 ± 0.06
Cx46 A14V (n=4)	+	1.01 ± 0.08	0.24 ± 0.04	35.1 ± 4.2	0.19 ± 0.14
	-	1.00 ± 0.08	0.15 ± 0.04	37.1 ± 3.0	0.14 ± 0.08
Cx46 Q15N (n=4)	+	1.10 ± 0.24	0.27 ± 0.12	37.3 ± 12.4	0.06 ± 0.04
	-	1.04 ± 0.16	0.25 ± 0.08	32.3 ± 7.8	0.09 ± 0.06

Data is presented as mean ± SD and V<sub>0</sub> are absolute values. Student's t-test was used to compare the Boltzmann fitting parameters of each variants against those of wildtype at the same V<sub>j</sub> polarity. No parameter showed statistically significant differences between each variant and wildtype connexin. N/A, not applicable.

**Table 2-2:** Boltzmann fitting parameters for the GJs of Cx50 and its variants.

<b>GJs</b>	<b>V<sub>j</sub> polarity</b>	<b>G<sub>max</sub></b>	<b>G<sub>min</sub></b>	<b>V<sub>0</sub></b>	<b>A</b>
Cx50 (n=6)	+	1.06 ± 0.22	0.20 ± 0.15	41.5 ± 11.8	0.07 ± 0.05
	-	1.10 ± 0.22	0.25 ± 0.15	43.6 ± 11.8	0.07 ± 0.05
Cx50 I10L (n=4)	+	1.03 ± 0.08	0.22 ± 0.04	33.0 ± 5.0	0.11 ± 0.04
	-	1.00 ± 0.10	0.22 ± 0.06	33.7 ± 4.2	0.17 ± 0.10
Cx50 E13N (n=3)	+	1.03 ± 0.27	0.16 ± 0.12	33.2 ± 6.9	0.1 ± 0.17
	-	1.03 ± 0.29	0.29 ± 0.14	30.0 ± 11.7	0.1 ± 0.14
Cx50 V14A (n=4)	+	0.95 ± 0.10	0.23 ± 0.08	45.4 ± 6.8	0.13 ± 0.10
	-	0.97 ± 0.12	0.23 ± 0.08	37.8 ± 5.8	0.14 ± 0.14
Cx50 N15Q (n=5)	+	1.05 ± 0.3	0.23 ± 0.13	37.1 ± 12.5	0.08 ± 0.07
	-	1.05 ± 0.3	0.18 ± 0.11	30.6 ± 11.7	0.09 ± 0.09

Data is presented as mean ± SD and V<sub>0</sub> are absolute values. Student's t-test was used to compare the Boltzmann fitting parameters of each variants against those of wildtype at the same V<sub>j</sub> polarity. No parameter showed statistically significant differences between each variant and wildtype connexin.

### 2.4.3 Unitary channel conductance of homotypic GJs of Cx46 and Cx50 NT variants.

To study how each Cx46 or Cx50 NT point variant affecting the rate of ion permeation in individual GJ channels, we recorded unitary channel currents (i<sub>js</sub>) in poorly coupled cell pairs at different V<sub>js</sub>. Typical i<sub>js</sub> from cell pairs expressing wildtype Cx46 or Cx50 showed increasing amplitudes as a function of increasing V<sub>js</sub> (Fig. 2-7A). The first ~2 s of the i<sub>js</sub> (rectangle areas outlined at the beginning of i<sub>js</sub>) were used to generate an all

point histogram (grey lines), which was fitted by two or more Gaussian functions (smooth black lines) to measure  $i_j$  (Fig. 2-7B). The  $i_j$  amplitudes at the main open state, fully closed state, as well as in some cases subconductance states could be identified. The  $i_j$  amplitudes of the main open state were plotted at the tested  $V_j$ s (Fig. 2-7C), and linear regression of the  $i_j - V_j$  plot was used to obtain the slope unitary channel conductance ( $\gamma_j$ ). The average slope  $\gamma_j$  of Cx46 GJ is  $192 \pm 5$  pS ( $n = 5$ ), whereas the average slope  $\gamma_j$  of Cx50 GJ is  $220 \pm 7$  pS ( $n = 5$ ),  $**p = 0.006$ .

Representative unitary channel currents ( $i_j$ s) of all the NT point variants at the 10<sup>th</sup>, 13<sup>th</sup>, 14<sup>th</sup>, and 15<sup>th</sup> positions of Cx46 (left panel) and Cx50 (right panel). In most cases, the  $i_j$ s showed higher open probability ( $P_{open}$ ) for the main open state at  $V_j$  of 40 mV than those at higher absolute  $V_j$ s (60 or 80 mV). During the larger  $V_j$  pulses (60 or 80 mV), both residual state (open arrows) and fully closed state (solid arrows) were observed (Fig. 2-8). All point histograms and Gaussian function fits were used to measure the amplitudes of  $i_j$ s at main open state for each tested  $V_j$ s (data not shown). The linear  $i_j - V_j$  plot for each of the Cx46 variants was used to obtain the slopes ( $\gamma_j$ s) and plotted together with the wildtype Cx46 slope  $\gamma_j$  after linear regression (Fig. 2-9A1). The slopes ( $\gamma_j$ ) from the Cx46 N13E and A14V were significantly decreased compared to the slope ( $\gamma_j$ ) from wildtype Cx46  $\gamma_j$  ( $93 \pm 17$  pS for N13E,  $**p = 0.001$  and  $94 \pm 11$  pS for A14V,  $***p < 0.001$ ). Similarly, the  $i_j - V_j$  plot for each of the Cx50 variants was generated and linear regression was used to obtain the slopes ( $\gamma_j$ s). The wildtype Cx50 slope ( $\gamma_j$ ) was used as a direct comparison to the variants (Fig. 2-9A2). The slope ( $\gamma_j$ ) of Cx50 E13N and N15Q GJs variants were significantly decreased compared to the wildtype Cx50 GJ ( $193 \pm 17$  pS for E13N,  $*p = 0.017$ ; and  $162 \pm 14$  pS for N15Q,  $**p = 0.002$ ).

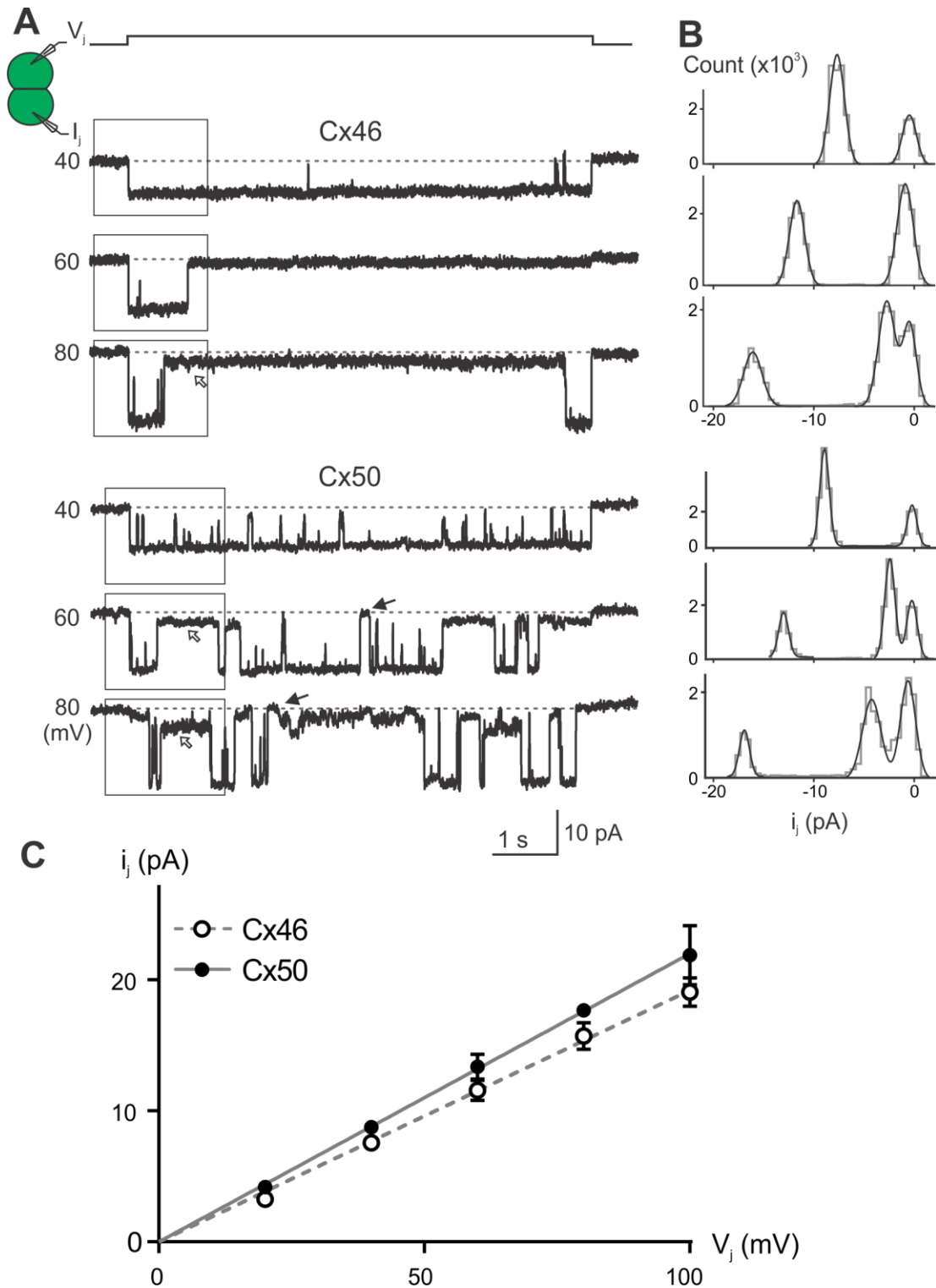


**Figure 2-7:** Unitary channel properties for wildtype Cx46 and Cx50 GJs. (A) Single channel currents ( $i_j$ s) recorded as a response to the administration of positive  $V_j$  pulses ( $+V_j$ ) as indicated. After the channels are fully open, they go to either subconductance

state (open arrows) or to fully closed state (solid arrows). Rectangle areas outlined represent the region used to create the corresponding all-point histograms shown on the right for each  $V_j$ . (B) All point histogram (grey lines) and Gaussian fits (smooth black lines) for  $i_j$ s of Cx46 and Cx50 at 40, 60, and 80 mV  $V_j$  pulses. They show the  $i_j$  amplitude at the main open state and fully closed state. Subconductance states were also identified at some  $V_j$ s. (C) Scatter plot of  $i_j$ s amplitude at the main open state for the entire tested range of  $V_j$ s. Linear regression of each  $i_j - V_j$  plot was used to obtain the slope which represents slope unitary channel conductance ( $\gamma_j$ ) for Cx46 or Cx50. For Cx46 GJ, the slope  $\gamma_j = 192 \pm 5$  pS ( $n = 5$ ) and for Cx50, the slope  $\gamma_j = 220 \pm 7$  pS ( $n = 5$ ).

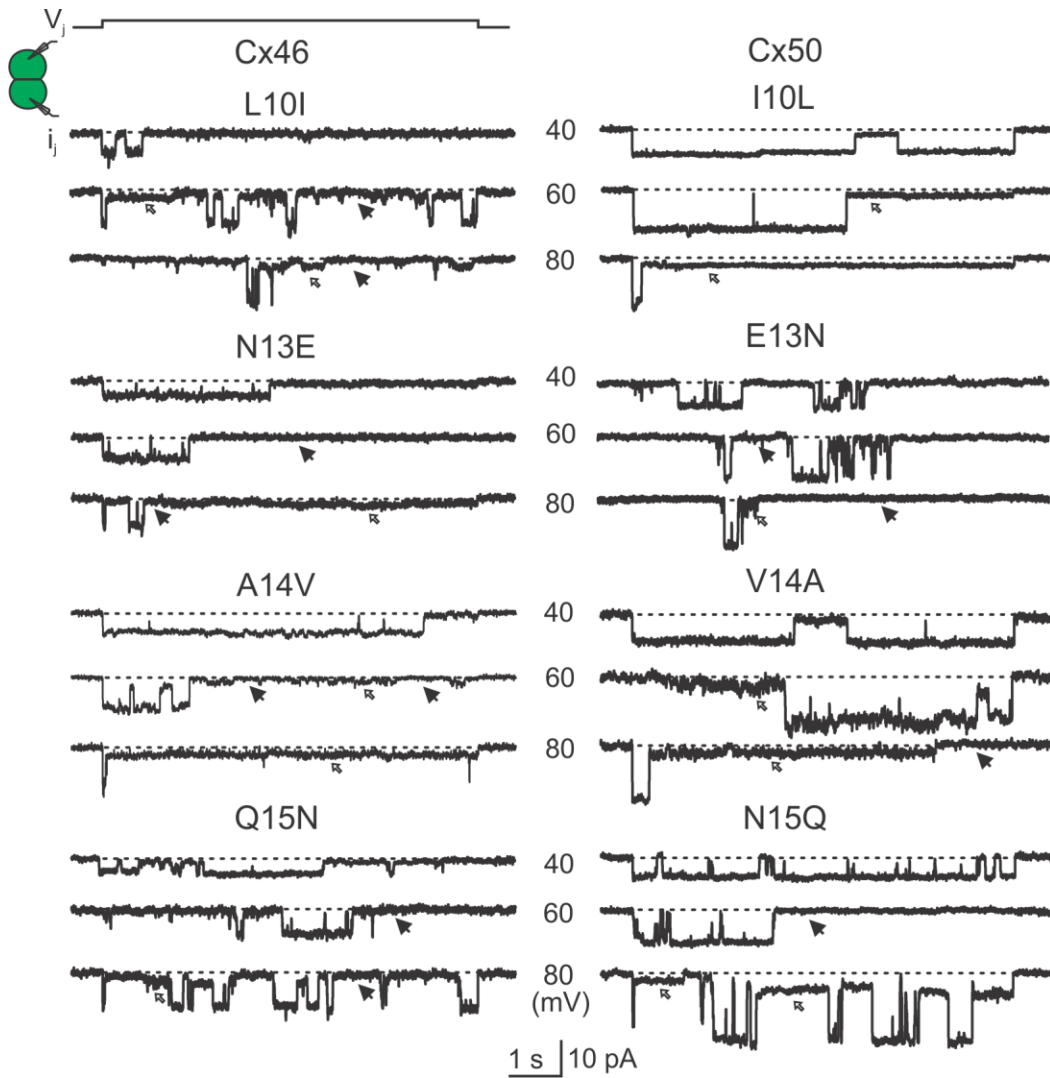


**Figure 2-8:** Single channel currents ( $i_{js}$ ) recorded in response to the indicated  $V_{js}$ . Representative  $i_{js}$  are shown for the homotypic GJs formed by Cx46 NT variants (left panels) or Cx50 NT variants (right panels). In addition to fully open state, subconductance (open arrows) and fully closed state (solid arrows) were also observed for most of  $i_{js}$ .

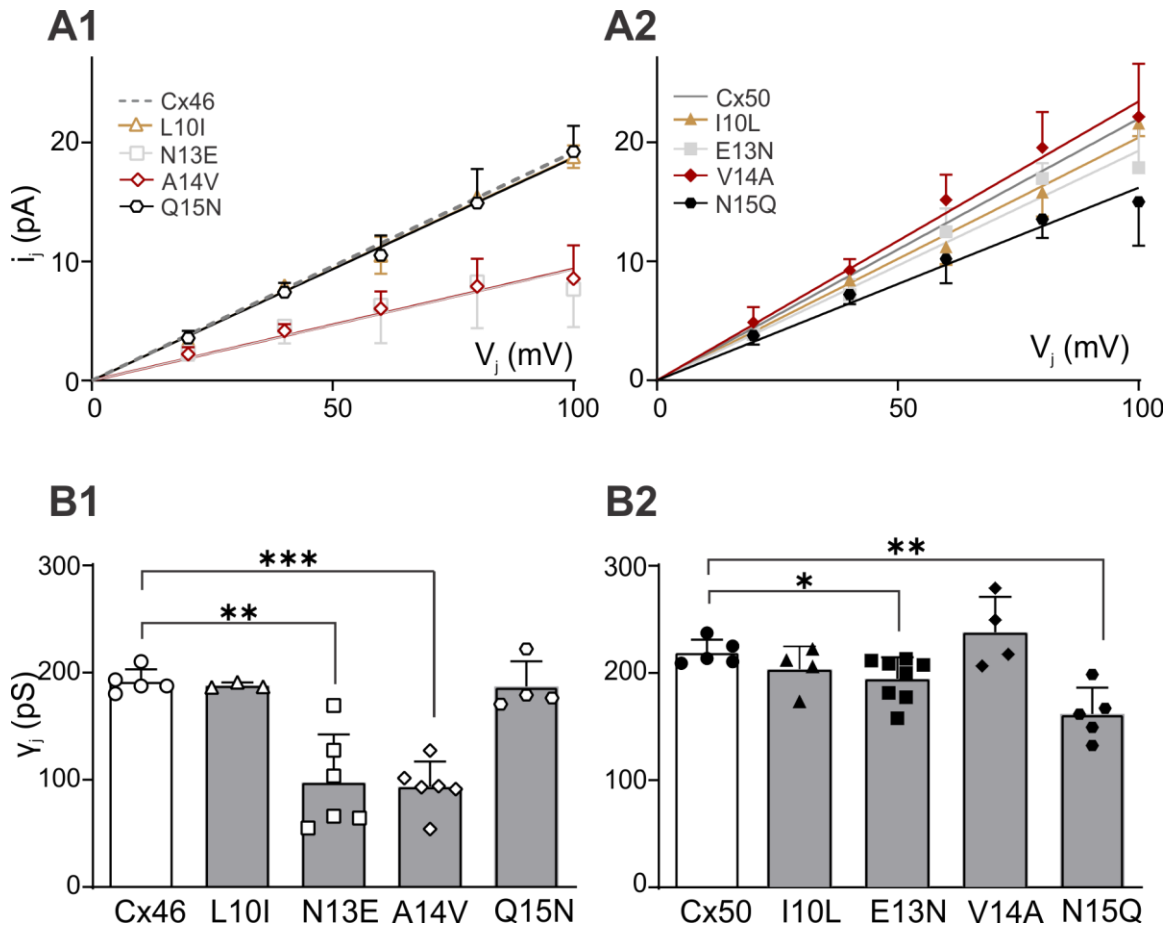


**Figure 2-9:** Unitary channel properties of homotypic GJs of Cx46 L10I, N13E, A14V, Q15N and Cx50 I10L, E13N, V14A, N15Q variants. (A) Scatter plot of  $i_j$ s amplitude at the main open state for the entire tested range of  $V_j$ s. Linear regression was used to obtain the slope which represents slope unitary channel conductance ( $\gamma_j$ ) for each variant. The dashed and solid gray lines represent the slope  $\gamma_j$ s of Cx46 and Cx50, respectively. The slope  $\gamma_j$  of Cx46 L10I is  $188 \pm 6$  pS ( $n = 3$ ), N13E  $\gamma_j$  is  $93 \pm 17$  pS ( $n = 6$ ), A14V  $\gamma_j$  is  $94 \pm 11$  pS ( $n = 6$ ), Q15N  $\gamma_j$  is  $187 \pm 10$  pS ( $n = 4$ ), Cx50 I10L  $\gamma_j$  is  $204 \pm 10$  pS ( $n = 4$ ), E13N  $\gamma_j$  is  $193 \pm 17$  pS ( $n = 8$ ), V14A  $\gamma_j$  is  $234 \pm 12$  pS ( $n = 4$ ), and N15Q  $\gamma_j$  is  $162 \pm 14$  ( $n = 5$ ). (B) Bar graphs for direct comparison of slope  $\gamma_j$ s of tested Cx46 (B1) and Cx50 (B2) variants. Cx46 N13E and A14V as well as Cx50 E13N and N15Q showed significantly lower  $\gamma_j$  compared to their corresponding wildtype. Unpaired Two-Samples T-test was used to compare each variant to corresponding wildtype.

#### 2.4.4 Homology modeling of selected Cx46 and Cx50 variants.

To start to explore structural mechanistic insights of our experimental results, homology models were developed for several variants with the most drastic changes. For example, Cx46 N13E was selected as its GJs showed significantly lower coupling%, reduced  $G_j$  in coupled cell pairs, and a large reduction in  $\gamma_j$ . The homology model of Cx46 N13E showed that E13 could have an occasional intra-subunit salt-bridge interaction with R9 as shown in Fig. 2-10A. The probability of this interaction as shown in Fig. 2-10A is not very high (only one E13 out of 6 interacts with R9), but we believe that this interaction is pulling the R9 toward the cytosol direction which could destabilize the NT from the open conformation to promote GJ closure or a reduced permeation passage. This could be partially contributed to our observed reduction in coupling%,  $G_j$ , and  $\gamma_j$ . We could not rule out other possibilities at this time.

Cx46 L10I is the only variant that caused large changes in its GJ  $V_j$ -gating. A simple exchange of this residue on Cx46 structure model (7JKC) resulted in a steric clash between I10 and L90 on the M2 domain (Fig. 2-10B), suggesting that these residues could play a role in maintaining normal  $V_j$ -gating properties. While the mirroring variant, Cx50 I10L, on Cx50 GJ structure (7JJP) did not show any steric clash and their  $V_j$ -gating properties appeared to be similar as the wildtype Cx50 GJ (Fig. 2-10B, see also Fig. 2-6).

Another interesting pair of variants are on hydrophobic residues, i.e., Cx46 A14V and Cx50 V14A. In the wildtype Cx46 and Cx50 the 14<sup>th</sup> residue packed tightly with two residues (89<sup>th</sup> and 93<sup>rd</sup>) in M2 domain to have hydrophobic interactions as shown in Fig. 2-10C. When valine is introduced in Cx46 (A14V), the larger side chain of valine produced a steric clash with T89 (Fig. 2-10C), which is likely to destabilize the NT domain, possibly pushing it into the GJ pore to reduce the pore size leading to a reduced  $G_j$  and  $\gamma_j$ . The mirror variant, Cx50 V14A, displayed no steric clash (Fig. 2-10C) and the NT domain could be packed closer to the M2 and could widen the GJ pore diameter. Such widening of the GJ pore might not be happening in the functional GJ channels, as we did not observe any predicted increase in the single channel conductance and the  $G_j$  of Cx50 V14A was also similar to that of Cx50.



To further study the importance of the hydrophobic interactions between the A14/V14 with the 89<sup>th</sup> or 93<sup>rd</sup> residues in the M2 domain, we also modeled variants at the 89<sup>th</sup> position in Cx46 and Cx50. Simply mutating the 89<sup>th</sup> residue on Cx46 or Cx50 GJ model predicted that Cx50 S89T caused a steric clash with the V14 of the same subunit, while the Cx46 T89S did not lead to any steric clash as A14 and S89 are both with small side chains. We then generated Cx50 S89T variant construct and expressed in N2A cells for dual patch clamp analysis. Our experimental result is shown in Fig. 2-11. Cx50 S89T failed to form functional GJ channels as both coupling% and  $G_j$  were significantly reduced to a minimum level comparing to wildtype Cx50 GJs. This result and our results on variants on 14<sup>th</sup> residues support the structure models on an important role of packing interactions between the 14<sup>th</sup> residue and the M2 residues in Cx46 and Cx50 GJs. Additional experiments are required to further validate these models.

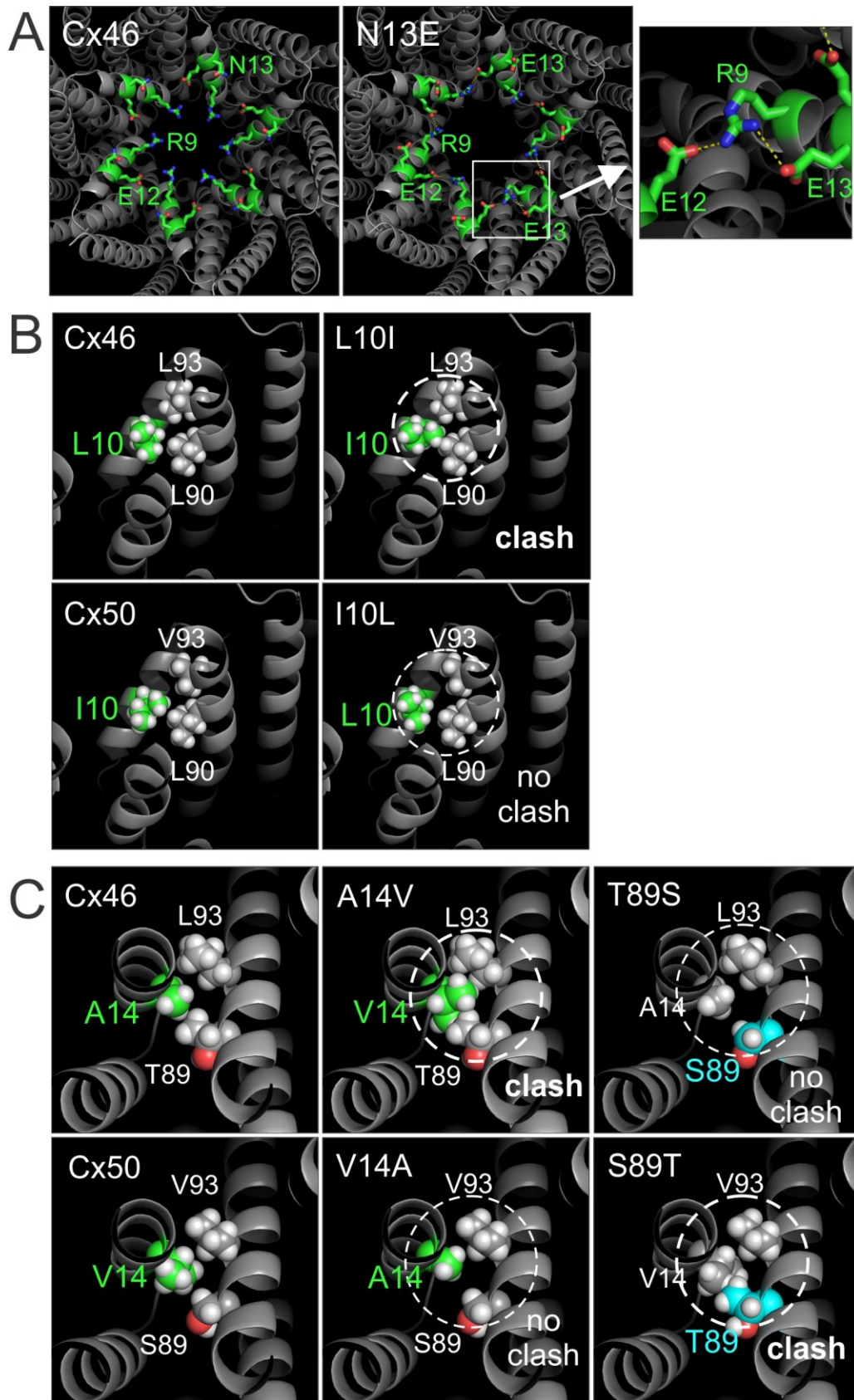


**Figure 2-10:** Structural models for selected variant GJs. (A) Cx46 GJ model determined by Cryo-EM (PDB: 7JKC) is shown on the left panel with a viewing angle facing the pore entrance. Homology model of Cx46 N13E is shown in the middle panel to show R9 and E12 frequently interact one another forming salt-bridges. On one occasion, the side chain of E13 also interact with the side chain of R9 of the same subunit to form salt bridge interactions (see enlarged view on the right panel). (B) A zoomed in view on Cx46 and Cx50 to highlight the interactions of the 10<sup>th</sup> residue with 90<sup>th</sup> and 93<sup>rd</sup> residues on the M2 domain (left panels). Cx46 L10I caused a steric clash between I10 and L90, while the Cx50 I10L did not lead to any steric clash with L90 or V93 (right panels). (C) A zoomed in view on Cx46 and Cx50 to highlight the interactions of the 14<sup>th</sup> residue with 89<sup>th</sup> and 93<sup>rd</sup> residues on the M2 domain (left panels). Cx46 A14V caused a steric clash between V14 and T89, while the Cx50 V14A did not lead to any steric clash at the equivalent residue (middle panels). Similarly, Cx50 S89T caused a steric clash with V14, while no clash was observed with Cx46 T89S (right panels).

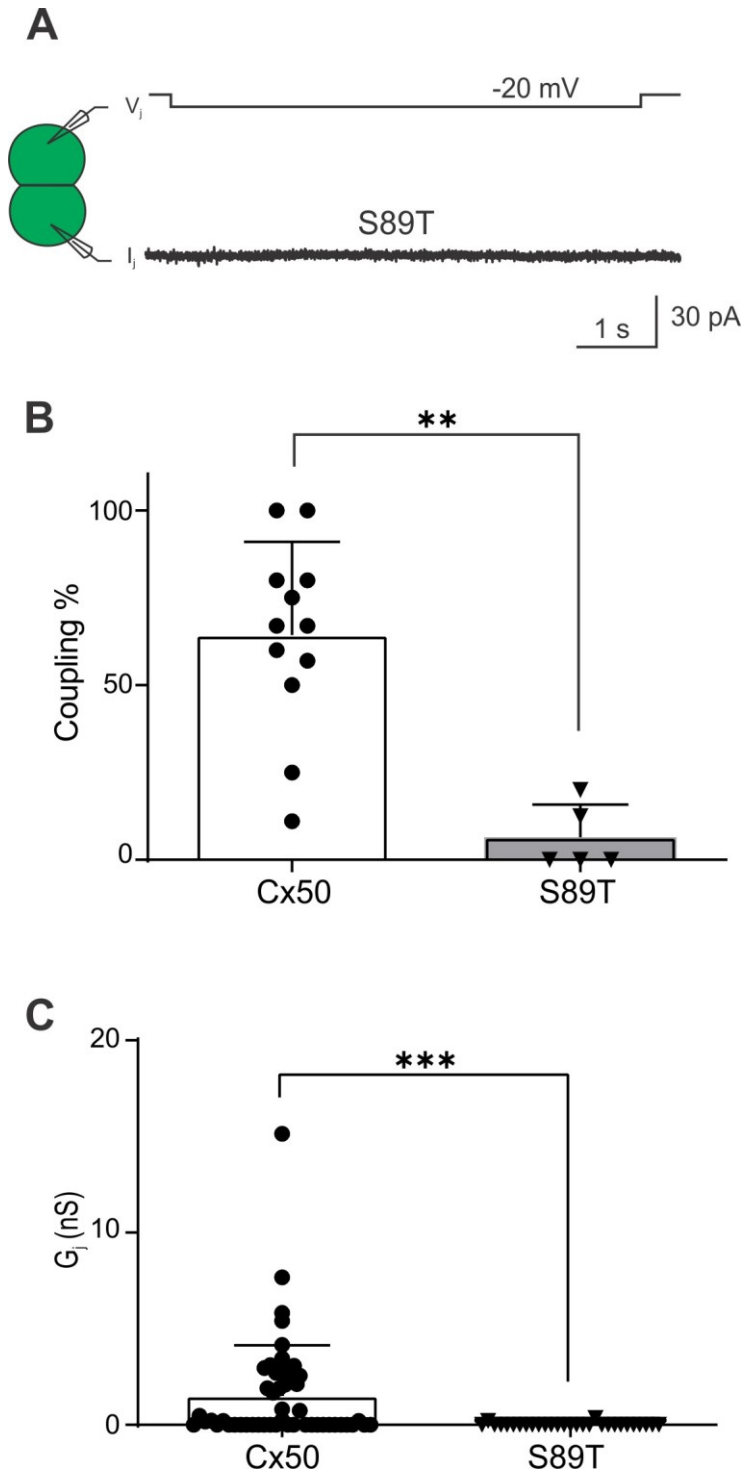


**Figure 2-11: Cx50 S89T failed to form functional GJs.** A. A representative  $I_j$  was recorded from a cell pair expressing Cx50 S89T. No current response was detected with a  $V_j$  pulse of 20 mV indicating S89T failed to form any functional GJs. B, C, summarized bar graphs to show coupling% and  $G_j$  of Cx50 S89T. In both cases, the S89T showed a

significantly reduction in coupling% (\*\*p = 0.001 with Mann-Whitney test) and  $G_j$  (\*\*\*)  $p < 0.001$  with Mann-Whitney test).

## 2.5 Discussion

Recently, atomic resolution (1.9 Å) structures on native Cx46 and Cx50 GJs were resolved in an open channel conformation (Flores et al., 2020), providing excellent templates for structure-function studies on these two GJs. These structure models proposed a novel network of intra- and inter-subunit hydrophobic packing interactions as the key mechanism anchoring the NT domain to the M1 and M2 domains, stabilizing the GJ channel in an open conformation. Our study aimed to examine several individual residues in the NT domain, including hydrophobic residues on the 10<sup>th</sup> and 14<sup>th</sup> positions, of these two lens connexins for their roles in GJ function, gating properties, and the single channel conductance ( $\gamma_j$ ). We engineered eight-point variants at the 10<sup>th</sup>, 13<sup>th</sup>, 14<sup>th</sup>, and 15<sup>th</sup> positions of NT domain, in which one amino acid residue was exchanged between Cx46 and Cx50. Our results show that all the NT variants were able to form functional GJs in our model cells (N2A), though the Cx46 N13E GJs showed a reduced coupling% and conductance. Conservative exchange of hydrophobic residues, such as L10I and A14V, in Cx46 showed a profound change in either  $V_j$ -gating or single channel conductance, respectively, indicating these hydrophobic residues are very important in  $V_j$ -gating and the rate of ion permeation. Looking into the GJ structures of these connexins and homology models of the NT variants, steric clash could be identified on Cx46 L10I and A14V with residues on M2. Interestingly, mutating one of the A14/V14 interacting residues in the M2 domain of Cx50, S89T (with a larger side chain), leads to a similar steric clash in the structure model and more importantly this variant failed to form functional GJs in our model cells. This study together with our previous study on switching the entire NT domain between these two lens connexins (Yue et al., 2021) support the newly proposed model that hydrophobic packing interactions between the NT and M2 domain play an important role in stabilizing the NT domain in an open channel conformation,  $V_j$ -gating, and unitary channel conductance in Cx46, Cx50, and possibly other connexin GJs.

Sheep connexins were selected to better align our functional data with the resolved high resolution GJ structure models (Myers et al., 2018, Flores et al., 2020). Sheep and human show 85% overall and 96% structure-resolved domain sequence identity for Cx50, and 67% overall and 95% structure-resolved domain sequence identity for Cx46. Similarly, sheep Cx46 and Cx50 also show high sequence identity with mouse orthologs. More importantly the NT domains and those residues in the M2 (89<sup>th</sup>, 90<sup>th</sup>, and 93<sup>rd</sup>) interacting with 10<sup>th</sup> and 14<sup>th</sup> residues in the NT of Cx46 or Cx50 are 100% identical among sheep, mouse, and human. Thus, we believe that sheep Cx46 and Cx50 are excellent models for the corresponding orthologs from human, rodents, or possibly other species.

Based on the cryo-EM structure models of Cx46 and Cx50 GJs, a large portion of the NT domain (4<sup>th</sup> – 17<sup>th</sup> residue) forms an  $\alpha$ -helix structure with hydrophobic residues facing M1/2 domains and hydrophilic residues facing the pore. The hydrophobic residues in the NT  $\alpha$ -helix showed novel inter- and intra- subunit interactions with hydrophobic or polar residues on M1/2 domains (Flores et al., 2020, Myers et al., 2018), including the 10<sup>th</sup> and 14<sup>th</sup> residues in the NT as shown in Fig. 2-10. However, in the Cx26 GJ crystal structure, only a small portion of NT domain (5<sup>th</sup> – 10<sup>th</sup> residue) formed  $\alpha$ -helix structure, and the equivalent residues in the Cx26 structure adopted a very different orientation. For example, the hydrophobic residue, I9 of Cx26 (equivalent to 10<sup>th</sup> residue in Cx46 and Cx50) is directly facing the pore and another hydrophobic residue V13 (equivalent to 14<sup>th</sup> residue in Cx46 and Cx50) is at least 4 Å away from any residue on the M2 domain (Maeda et al., 2009); in both cases they are unlikely to form any intra-subunit packing interactions. Molecular dynamic simulations on Cx46 and Cx50 GJ models found that these structures are stable in the proposed open conformation due to the extensive hydrophobic packing interactions between the NT and M1/2 domains, unlike that of Cx26 GJ structure (very unstable in the open conformation) (Myers et al., 2018). It is interesting to note that molecular dynamic simulations on chimeras of Cx46 and Cx50 with swapped NT domains showed a large increase in NT domain instability in Cx46 50NT GJ (a chimera with Cx50 NT domain replacing that of Cx46) due to steric clash of hydrophobic residues on the NT domain, which correlated with a complete loss of GJ function (Yue et al., 2021). These observations indicate an important role of hydrophobic

packing interactions between NT and M1/2 in stabilizing the NT domain in open conformation.

Our current study further tested several different residues individually in the NT domains of these two connexins. Consistent with our previous study, we identified that hydrophobic residues at 10<sup>th</sup> and 14<sup>th</sup> residues in Cx46 are leading to steric clash with residues on M2 domain and altering the GJ structure. Surprisingly, single mutant variants were still able to form functional GJs, but with altered  $V_j$ -gating (L10I) or  $\gamma_j$  (A14V). Additionally, our designed variant S89T in Cx50 also produced steric clash between V14 and T89, which resulted in a complete loss of GJ function (Fig. 2-11), demonstrating the importance of the intermolecular stabilizing interactions between NT and M2 domain for GJ function, gating properties and ion permeation. Additional lines of evidence support important functional roles of the hydrophobic residues in the NT domain of Cx46 and Cx50. First, several congenital cataract linked missense mutations occur on these hydrophobic residues, such as L11S in Cx46 as well as W4R and L7P in Cx50 (Hansen et al., 2006, Tong et al., 2013, Javadiyan et al., 2018, Mackay et al., 2014, Zhang et al., 2018). It is interesting to mention that L11S failed to form functional GJs in xenopus oocytes when paired homotypically and did not show any hemichannel activity as well (Tong et al., 2013). Second, hydrophobic residues are highly conserved in Cx46 and Cx50 as well as among  $\alpha$  and other families of connexins and the equivalent hydrophobic residue positions are almost all able to form amphipathic  $\alpha$ -helix to likely interact with their M1/2 domains (see Fig. 3-2). Mutations of the hydrophobic NT residues of a  $\beta$ -connexin, Cx32, including, W3D, L6D, L9D, and L10D all resulted in non-functional GJs (Purnick et al., 2000). These data collectively emphasize a critical role played by the hydrophobic residues of NT domain in determining GJ channel function and its properties.

In addition to hydrophobic residues in determining Cx46 GJ functional properties, Cx46 N13E showed a significantly decreased coupling% as well as macroscopic and unitary channel conductance in the present study. Our homology model on Cx46 N13E showed that this mutation altered the network of intra- and inter-subunit salt-bridge interactions. Some of these interactions including the R9 with a neighboring subunit E12 salt-bridge

were frequent and were also predicted to exist during molecular dynamic simulation on wildtype Cx46 GJs (Yue et al., 2021), but a rare frequency intra-subunit salt-bridge interaction between R9 and E13 was observed (Fig. 2-10A). This non-covalent salt-bridge interaction could pull R9 towards the cytosol, which could destabilize the open conformation of the NT domain to trigger/facilitate the initial step of GJ closing. We cannot rule out that other structural changes associated with N13E, including subunit folding or additional changes in interacting partners, could also play a role in observed reduction in coupling%,  $G_j$ , and  $\gamma_j$ . Reduction of  $\gamma_j$  in Cx46 N13E is somewhat surprising, as we predicted this variant would increase the net negative charge at the GJ pore entrance and lead to enhanced cation concentration; thereby increase rate of permeation of this cation preferred channel. Previous studies by our group on Cx46 and Cx50 and its variant GJs displayed higher  $\gamma_j$  with increasing negative charge of the NT, M1, E1 domains (all pore lining domains) (Xin and Bai, 2013, Tong et al., 2014, Tejada et al., 2018) or decreasing in positive charge in the NT like Cx46 R9N (Yue et al., 2021). Apparently for these two cation preferred GJ channels, higher net negative charge in pore lining residues would be predicted to increase the negativity of pore surface electrostatic potentials, which in general favor increasing local cation concentrations in the pore or the pore entrance area; both, in theory, should increase the rate of permeation or  $\gamma_j$ . In many of these variants the  $\gamma_j$  was indeed increased (Xin and Bai, 2013, Tong et al., 2014, Tejada et al., 2018, Yue et al., 2021). However, caution should be taken, as some additional physical changes are also associated with these charged residue variants. The side chain length (or size) could reduce the pore diameter or establish additional intra- and inter-subunit interactions to alter the permeation passage structure and properties, thereby changing  $\gamma_j$  or other gating properties. These additional changes could play a role in our observed reduction in  $\gamma_j$  in Cx46 N13E and one of our previously studied Cx50 variants, D3E (Xin et al., 2012).

Another example of a changed network of intra- and inter-subunit interactions by a missense mutation in a pore lining residue is the congenital cataract-linked mutation in Cx50, T39R. The T39R Cx50 hemichannels showed partial loss of  $V_j$  gating, and molecular dynamic simulations showed changes in multiple electrostatic salt-bridge



interactions by the introduced R39, including neutralizing the putative voltage sensing residue D3, as well as a newly established interaction with E42, which could participate in loop gating (Tong et al., 2021). Steric factors might also play a role in the reduced coupling and conductance of N13E observed in the present study, as glutamic acid has bulkier side chain than the original asparagine. Similarly, Cx45 R8D and R8E variants were unable to form functional GJs while insignificant changes in  $V_j$ -gating or  $\gamma_j$  were reported for the Cx50 G8E mutant, despite addition of negatively charged residues (Santos-Miranda et al., 2020, Xin et al., 2012).

Our findings suggest that both 13<sup>th</sup> and 14<sup>th</sup> positions are important determinants of Cx46 GJs function and, alongside the 9<sup>th</sup> position, might be responsible for the loss of function in the previously studied Cx46-50NT chimera. The 10<sup>th</sup> residue also plays a critical role in the maintenance of  $V_j$ -gating based on the data of the present study. For Cx50 GJs, it appears that the 13<sup>th</sup> and 15<sup>th</sup> residues (besides the 9<sup>th</sup> position) are also partially involved in the observed decrease in  $\gamma_j$  of Cx50-46NT, which demonstrated a crucial role in gating as well as  $\gamma_j$ . To sum up, our study concludes that, beside charge, side chain length as well as the location of amino acid residue relative to the pore and to the other neighboring domains influence their intra- and inter-subunit interactions, which affects the stability of GJ channel conformation and its gating and ion permeation.

## 2.6 References

- ABASCAL, F. & ZARDOYA, R. 2013. Evolutionary analyses of gap junction protein families. *Biochim. Biophys. Acta*, 1828, 4-14.
- BAI, D. & CAMERON, J. A. 2016. Patch clamp analysis of gap junction channel properties. *Gap Junction Channels and Hemichannels*. CRC Press.
- BENNETT, B. C., PURDY, M. D., BAKER, K. A., ACHARYA, C., MCINTIRE, W. E., STEVENS, R. C., ZHANG, Q., HARRIS, A. L., ABAGYAN, R. & YEAGER, M. 2016. An electrostatic mechanism for Ca(2+)-mediated regulation of gap junction channels. *Nat Commun*, 7, 8770.
- BUKAUSKAS, F. F. & VERSELIS, V. K. 2004. Gap junction channel gating. *Biochim. Biophys. Acta*, 1662, 42-60.
- BUKAUSKAS, F. F. & WEINGART, R. 1994. Voltage-dependent gating of single gap junction channels in an insect cell line. *Biophys. J.*, 67, 613-25.
- FLORES, J. A., HADDAD, B. G., DOLAN, K. A., MYERS, J. B., YOSHIOKA, C. C., COPPERMAN, J., ZUCKERMAN, D. M. & REICHOW, S. L. 2020. Connexin-46/50 in a dynamic lipid environment resolved by CryoEM at 1.9 Å. *Nat Commun*, 11, 4331.
- GERIDO, D. A. & WHITE, T. W. 2004. Connexin disorders of the ear, skin, and lens. *Biochim. Biophys. Acta*, 1662, 159-70.
- GOLDBERG, G. S., VALIUNAS, V. & BRINK, P. R. 2004. Selective permeability of gap junction channels. *Biochim. Biophys. Acta*, 1662, 96-101.
- GONZÁLEZ, D., GÓMEZ-HERNÁNDEZ, J. M. & BARRIO, L. C. 2007. Molecular basis of voltage dependence of connexin channels: an integrative appraisal. *Prog. Biophys. Mol. Biol.*, 94, 66-106.
- GOODENOUGH, D. A., GOLIGER, J. A. & PAUL, D. L. 1996. Connexins, connexons, and intercellular communication. *Annual review of biochemistry*, 65, 475-502.
- GOODENOUGH, D. A. & PAUL, D. L. 2009. Gap junctions. *Cold Spring Harb. Perspect. Biol.*, 1, a002576.
- HANSEN, L., YAO, W., EIBERG, H., FUNDING, M., RIISE, R., KJAER, K. W., HEJTMANCIK, J. F. & ROSENBERG, T. 2006. The congenital "ant-egg" cataract phenotype is caused by a missense mutation in connexin46. *Mol. Vis.*, 12, 1033-9.
- JASSIM, A., AOYAMA, H., YE, W. G., CHEN, H. & BAI, D. 2016. Engineered Cx40 variants increased docking and function of heterotypic Cx40/Cx43 gap junction channels. *J. Mol. Cell. Cardiol.*, 90, 11-20.

- JAVADIYAN, S., LUCAS, S. E. M., WANGMO, D., NGY, M., EDUSSURIYA, K., CRAIG, J. E., RUDKIN, A., CASSON, R., SELVA, D., SHARMA, S., LOWER, K. M., MEUCKE, J. & BURDON, K. P. 2018. Identification of novel mutations causing pediatric cataract in Bhutan, Cambodia, and Sri Lanka. *Mol Genet Genomic Med*, 6, 555-64.
- KHAN, A. K., JAGIELNICKI, M., MCINTIRE, W. E., PURDY, M. D., DHARMARAJAN, V., GRIFFIN, P. R. & YEAGER, M. 2020. A Steric "Ball-and-Chain" Mechanism for pH-Mediated Regulation of Gap Junction Channels. *Cell Rep.*, 31, 107482.
- KRONENGOLD, J., SRINIVAS, M. & VERSELIS, V. K. 2012. The N-terminal half of the connexin protein contains the core elements of the pore and voltage gates. *J. Membr. Biol.*, 245, 453-63.
- KWON, T., HARRIS, A. L., ROSSI, A. & BARGIELLO, T. A. 2011. Molecular dynamics simulations of the Cx26 hemichannel: evaluation of structural models with Brownian dynamics. *The Journal of general physiology*, 138, 475-93.
- LO, C. W. 2000. Role of gap junctions in cardiac conduction and development: insights from the connexin knockout mice. *Circulation research*, 87, 346-8.
- LUO, Y., ROSSI, A. R. & HARRIS, A. L. 2016. Computational Studies of Molecular Permeation through Connexin26 Channels. *Biophysical journal*, 110, 584-599.
- MACKAY, D. S., BENNETT, T. M., CULICAN, S. M. & SHIELS, A. 2014. Exome sequencing identifies novel and recurrent mutations in GJA8 and CRYGD associated with inherited cataract. *Hum Genomics*, 8, 19.
- MAEDA, S., NAKAGAWA, S., SUGA, M., YAMASHITA, E., OSHIMA, A., FUJIYOSHI, Y. & TSUKIHARA, T. 2009. Structure of the connexin 26 gap junction channel at 3.5 Å resolution. *Nature*, 458, 597-602.
- MAEDA, S. & TSUKIHARA, T. 2011. Structure of the gap junction channel and its implications for its biological functions. *Cellular and molecular life sciences : CMLS*, 68, 1115-29.
- MEŞE, G., RICHARD, G. & WHITE, T. W. 2007. Gap junctions: basic structure and function. *The Journal of investigative dermatology*, 127, 2516-24.
- MORENO, A. P., CHANSON, M., ELENES, S., ANUMONWO, J., SCERRI, I., GU, H., TAFFET, S. M. & DELMAR, M. 2002. Role of the carboxyl terminal of connexin43 in transjunctional fast voltage gating. *Circ. Res.*, 90, 450-7.
- MORENO, A. P., ROOK, M. B., FISHMAN, G. I. & SPRAY, D. C. 1994. Gap junction channels: distinct voltage-sensitive and -insensitive conductance states. *Biophys. J.*, 67, 113-9.

- MUSA, H., FENN, E., CRYE, M., GEMEL, J., BEYER, E. C. & VEENSTRA, R. D. 2004. Amino terminal glutamate residues confer spermine sensitivity and affect voltage gating and channel conductance of rat connexin40 gap junctions. *J. Physiol.*, 557, 863-78.
- MYERS, J. B., HADDAD, B. G., O'NEILL, S. E., CHOREV, D. S., YOSHIOKA, C. C., ROBINSON, C. V., ZUCKERMAN, D. M. & REICHOW, S. L. 2018. Structure of native lens connexin 46/50 intercellular channels by cryo-EM. *Nature*, 564, 372-377.
- NOURELDIN, M., CHEN, H. & BAI, D. 2018. Functional Characterization of Novel Atrial Fibrillation-Linked GJA5 (Cx40) Mutants. *Int. J. Mol. Sci.*, 19.
- ORELLANA, J. A., AVENDAÑO, B. C. & MONTERO, T. D. 2014. Role of connexins and pannexins in ischemic stroke. *Curr. Med. Chem.*, 21, 2165-82.
- PELLEGRINI-CALACE, M., MAIWALD, T. & THORNTON, J. M. 2009. PoreWalker: a novel tool for the identification and characterization of channels in transmembrane proteins from their three-dimensional structure. *PLoS computational biology*, 5, e1000440.
- PERACCHIA, C. & PERACCHIA, L. L. 2005. Inversion of both gating polarity and CO<sub>2</sub> sensitivity of voltage gating with D3N mutation of Cx50. *Am. J. Physiol. Cell Physiol.*, 288, C1381-9.
- PURNICK, P. E., OH, S., ABRAMS, C. K., VERSELIS, V. K. & BARGIELLO, T. A. 2000. Reversal of the gating polarity of gap junctions by negative charge substitutions in the N-terminus of connexin 32. *Biophys. J.*, 79, 2403-15.
- SANTOS-MIRANDA, A., CHEN, H., CHEN, R. C., ODOKO-ISHIMOTO, M., AOYAMA, H. & BAI, D. 2020. The amino terminal domain plays an important role in transjunctional voltage-dependent gating kinetics of Cx45 gap junctions. *J. Mol. Cell. Cardiol.*, 143, 71-84.
- SINYUK, M., MULKEARNS-HUBERT, E. E., REIZES, O. & LATHIA, J. 2018. Cancer Connectors: Connexins, Gap Junctions, and Communication. *Front. Oncol.*, 8, 646.
- SÖHL, G., MAXEINER, S. & WILLECKE, K. 2005. Expression and functions of neuronal gap junctions. *Nat. Rev. Neurosci.*, 6, 191-200.
- SRINIVAS, M., ROZENTAL, R., KOJIMA, T., DERMETZEL, R., MEHLER, M., CONDORELLI, D. F., KESSLER, J. A. & SPRAY, D. C. 1999. Functional properties of channels formed by the neuronal gap junction protein connexin36. *J. Neurosci.*, 19, 9848-55.
- TEJADA, M. G., SUDHAKAR, S., KIM, N. K., AOYAMA, H., SHILTON, B. H. & BAI, D. 2018. Variants with increased negative electrostatic potential in the Cx50

gap junction pore increased unitary channel conductance and magnesium modulation. *Biochem. J.*, 475, 3315-3330.

- TEUBNER, B., DEGEN, J., SÖHL, G., GÜLDENAGEL, M., BUKAUSKAS, F. F., TREXLER, E. B., VERSELIS, V. K., DE ZEEUW, C. I., LEE, C. G., KOZAK, C. A., PETRASCH-PARWEZ, E., DERMIETZEL, R. & WILLECKE, K. 2000. Functional expression of the murine connexin 36 gene coding for a neuron-specific gap junctional protein. *J. Membr. Biol.*, 176, 249-62.
- TONG, J.-J. & EBIHARA, L. 2006. Structural Determinants for the Differences in Voltage Gating of Chicken Cx56 and Cx45.6 Gap-Junctional Hemichannels. *Biophys. J.*, 91, 2142-2154.
- TONG, J. J., KHAN, U., HADDAD, B. G., MINOGUE, P. J., BEYER, E. C., BERTHOUD, V. M., REICHOW, S. L. & EBIHARA, L. 2021. Molecular mechanisms underlying enhanced hemichannel function of a cataract-associated Cx50 mutant. *Biophys. J.*, 120, 5644-5656.
- TONG, J. J., SOHN, B. C., LAM, A., WALTERS, D. E., VERTEL, B. M. & EBIHARA, L. 2013. Properties of two cataract-associated mutations located in the NH2 terminus of connexin 46. *Am. J. Physiol. Cell Physiol.*, 304, C823-32.
- TONG, X., AOYAMA, H., TSUKIHARA, T. & BAI, D. 2014. Charge at the 46th residue of connexin 50 is crucial for the gap-junctional unitary conductance and transjunctional voltage-dependent gating. *J. Physiol.*, 592, 5187-202.
- VEENSTRA, R. D., WANG, H. Z., BEYER, E. C., RAMANAN, S. V. & BRINK, P. R. 1994. Connexin37 forms high conductance gap junction channels with subconductance state activity and selective dye and ionic permeabilities. *Biophys. J.*, 66, 1915-28.
- VERSELIS, V. K., GINTER, C. S. & BARGIELLO, T. A. 1994. Opposite voltage gating polarities of two closely related connexins. *Nature*, 368, 348-51.
- VILLANELO, F., ESCALONA, Y., PAREJA-BARRUETO, C., GARATE, J. A., SKERRETT, I. M. & PEREZ-ACLE, T. 2017. Accessing gap-junction channel structure-function relationships through molecular modeling and simulations. *BMC Cell Biology*, 18, 5.
- WILDERS, R. & JONGSMA, H. J. 1992. Limitations of the dual voltage clamp method in assaying conductance and kinetics of gap junction channels. *Biophys. J.*, 63, 942-53.
- XIN, L. & BAI, D. 2013. Functional roles of the amino terminal domain in determining biophysical properties of Cx50 gap junction channels. *Front. Physiol.*, 4, 373.

- XIN, L., GONG, X. Q. & BAI, D. 2010. The role of amino terminus of mouse Cx50 in determining transjunctional voltage-dependent gating and unitary conductance. *Biophys. J.*, 99, 2077-86.
- XIN, L., NAKAGAWA, S., TSUKIHARA, T. & BAI, D. 2012. Aspartic acid residue D3 critically determines Cx50 gap junction channel transjunctional voltage-dependent gating and unitary conductance. *Biophys. J.*, 102, 1022-31.
- YUE, B., HADDAD, B. G., KHAN, U., CHEN, H., ATALLA, M., ZHANG, Z., ZUCKERMAN, D. M., REICHOW, S. L. & BAI, D. 2021. Connexin 46 and connexin 50 gap junction channel properties are shaped by structural and dynamic features of their N-terminal domains. *J. Physiol.*, 599, 3313-3335.
- ZHANG, L., LIANG, Y., ZHOU, Y., ZENG, H., JIA, S. & SHI, J. 2018. A Missense Mutation in GJA8 Encoding Connexin 50 in a Chinese Pedigree with Autosomal Dominant Congenital Cataract. *Tohoku J. Exp. Med.*, 244, 105-111.

## 3 Discussion

### 3.1 Overall study

We functionally characterize the gating and single channel properties of GJ variants at several positions of NT domains of Cx46 and Cx50 for which recent high-resolution structures have been recently resolved. These structures revealed that each NT domain of both connexin GJs adopted an amphipathic helical structure closely packing against M1 and M2 domains at the same or neighboring subunit. These interactions are mostly mediated by hydrophobic residues in NT and M1/2 domains and are believed to play a critical role in stabilizing the open state conformation of the GJ channels (Flores et al., 2020, Myers et al., 2018). Our electrophysiological recordings showed that Cx46 L10I, N13E, A14V, and Q15N as well as Cx50 I10L, E13N, V14A, and N15Q were all able to form functional GJs. The  $V_j$ -gating profile of the functional GJ channels show strong symmetrical  $V_j$ -dependent junctional current deactivation except for L10I which shows asymmetric gating. Single channel conductance ( $\gamma_j$ ) analysis revealed that both Cx46 N13E and A14V decreased  $\gamma_j$  markedly compared with Cx46  $\gamma_j$ . Homology structure model of A14V showed a steric clash between V14 and T89. To further test the importance of NT – M2 hydrophobic packing interaction, Cx50 S89T was designed, which also showed steric clash between the V14 and T89, and our experimental data found that this variant was unable to form functional GJ channels. In addition, Cx50 E13N and N15Q showed a small but significant decrease in  $\gamma_j$  compared with that of Cx50. In contrast, Cx46 L10I, Q15N, and Cx50 I10L, and V14A didn't modify  $\gamma_j$  as compared to their respective wildtype GJs.

### 3.2 Sequence alignment and design of variants

Single point variants at 10<sup>th</sup>, 13<sup>th</sup>, 14<sup>th</sup>, and 15<sup>th</sup> residue positions were generated based on the sequence alignment of the NT domains of Cx46 and Cx50 as shown in Fig. 3-1. Most amino acid residues are similar; however, the 9<sup>th</sup>, 10<sup>th</sup>, 13<sup>th</sup>, 14<sup>th</sup>, and 15<sup>th</sup> residues are different between these lens connexins. Among different residues, 9<sup>th</sup> and 13<sup>th</sup> residue

positions has different charge properties (R9 vs N9, and N13 vs E13 in Cx46 and Cx50, respectively), whereas the 10<sup>th</sup>, 14<sup>th</sup>, and 15<sup>th</sup> amino acid residues showed changes in side chain layout or size. To illustrate, leucine and isoleucine at 10<sup>th</sup> positions are hydrophobic residues with same size of side chain but different layout, while the alanine and valine at 14<sup>th</sup> position are hydrophobic residues with different in the side chain size. The 15<sup>th</sup> position has polar residues that are different in side chain size (Q15 vs N15, Fig. 3-1). Because switching the NT domain between Cx46 and Cx50 had resulted in loss of function (Cx46-50NT) or eliminated V<sub>j</sub>-gating and reduced  $\gamma_j$  (Cx50-46NT), we believe that NT domain is critical for the maintenance of channel's function, V<sub>j</sub>-gating, and  $\gamma_j$  (Yue et al., 2021). Despite that Cx46 and Cx50 share 80% of sequence identity, they vary in  $\gamma_j$  from 140 – 190 pS of Cx46 GJ to 200-220 pS of Cx50 GJ (Yue et al., 2021, Hopperstad et al., 2000, Tong et al., 2014). We believe that one or more of these different residues in the NT domain is/are contributing to such observed differences in the functional properties of chimeras and wildtype GJs. Previous study investigated the functional properties of 9<sup>th</sup> position by engineering two missense variants: Cx46 R9N and Cx50 N9R which did not fully explain these differences. Moreover, the functional role of individual hydrophobic residues at NT domain is still unclear. Consequently, to continue to study the roles of the remaining 4 different residues in the NT between Cx46 and Cx50, we generated point variants at the 10<sup>th</sup>, 13<sup>th</sup>, 14<sup>th</sup>, and 15<sup>th</sup> positions (Cx46 L10I, N13E, A14V, Q15N and Cx50 I10L, E13N, V14A, N15Q).



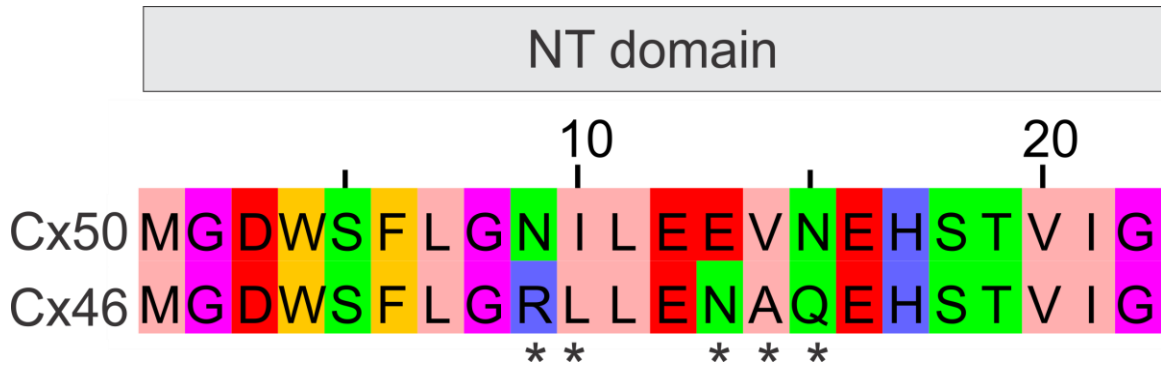
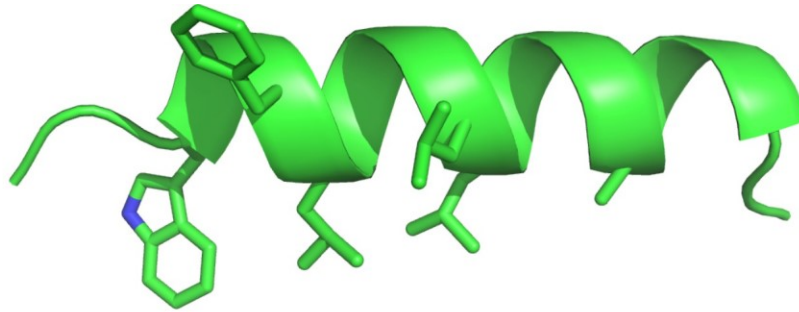


**Figure 3-1:** Sequence alignment of sheep Cx46 and Cx50 at the NT domain. Asterisks indicate different amino acids in the NT domain residue positions.

### 3.3 Functional characterization of NT variants of Cx46 and Cx50 GJs

Both Cx46 and Cx50 wildtype GJs showed prominent  $V_j$ -gating in the range of our tested  $V_j$ s that was well described by a two state Boltzmann equation at each  $V_j$  polarity similar to a previous study (Yue et al., 2021). A typical voltage-gating model for voltage-gated ion channels states that during the gating process, a change in voltage causes charge to migrate or dipoles (the voltage sensor) to reorient relative to the field, resulting in the channel closing or opening (Bezannilla, 2000). For GJ channels, the pore lining region of NT domain was proposed to be at least part of the  $V_j$ -gating voltage sensor, with  $V_j$ -gate closure triggered by voltage-sensing residues moving inward (toward the cytoplasm) (Bargiello et al., 2018, Purnick et al., 2000, Oh et al., 2004). The cryo-EM structure further supports this model as that NT domain folds into cytoplasmic vestibule, a position that could serve to sense changes in  $V_j$ . Cx46-L10I has asymmetric  $V_j$ -gating where gating is absent on one  $V_j$ -polarity. Because Leu and Ile are structural isomers, different in side-chain layout, the different orientation could affect the intra/inter-subunit interactions between NT and M1/2 (see Fig. 2-10) and thereby affecting the stability of the channel. Our homology model of L10I showed possible clash between I10 and L90 within the same subunit (Fig. 2-10) possibly destabilizing the open state conformation.

Consistent with the homology model structure of the nonfunctional Cx46-50NT chimera which showed a steric clash between A14 and T89 (Yue et al., 2021), our designed point variants Cx46 A14V and Cx50 S89T resulted in reduced  $G_j$  partially due to reduced  $\gamma_j$  and loss of function, respectively. We generated homology models of these two variants using higher resolution, 1.9 Å, and a steric clash was evident in both variant structure models. We also investigated the role of Cx46 L93V and Cx50 V93L because this residue is in close proximity to both 10<sup>th</sup> and 14<sup>th</sup> positions. Our preliminary data showed that both variants on 93<sup>rd</sup> position were functional with no apparent changes in  $V_j$ -gating or  $\gamma_j$  as compared to corresponding wildtypes, in congruent with homology structures of L10I and A14V which showed no clash between the introduced residue with that residue on 93<sup>rd</sup> position. Mutations in hydrophobic residues at NT domain of Cx46 and Cx50 GJs are associated with the development of cataracts. For example, L11S in Cx46 as well as W4R and L7P in Cx50 (Hansen et al., 2006, Tong et al., 2013, Zhang et al., 2018, Mackay et al., 2014, Javadiyan et al., 2018). Moreover, many ODDD-linked Cx43 variants L7V, L11I, L11F, L11P and G21R are also including changes of hydrophobic residues at the NT domain (Porntaveetus et al., 2017, Liu et al., 2001, Jamsheer et al., 2009, Paznekas et al., 2009, Kelly et al., 2006, Paznekas et al., 2003). Switching one residue in this domain often leads to changes to the GJ localization or function, which might play a role in cataract pathogenesis. Our research combines structural and functional data to provide mechanistic insights into how Cx46 and Cx50 GJs regulate ion permeation and gating, which could help explain the etiology of cataract-related connexin variations and possibly other connexin-linked illnesses. Hydrophobic residues in NT domains of all connexins are highly conserved as illustrated shown by their sequence logo in Fig. 3-2, suggesting that they may play a similar hydrophobic anchoring role in stabilizing GJ open conformation. In these hydrophobic residue positions (grey boxes), they are conserved to the same or other hydrophobic residues in almost every single connexin family. Only exceptions were observed on  $\beta$  connexins at 6<sup>th</sup> (with some polar residues) and  $\gamma$  connexins at 14<sup>th</sup> (sometimes with negatively charged glutamate, E) position equivalent residues (arrows in Fig. 3-2). Whether these hydrophobic residues are also play an anchoring NT domain in its open conformation are not yet investigated and would be an interesting topic for future studies.



Cx46 NT domain

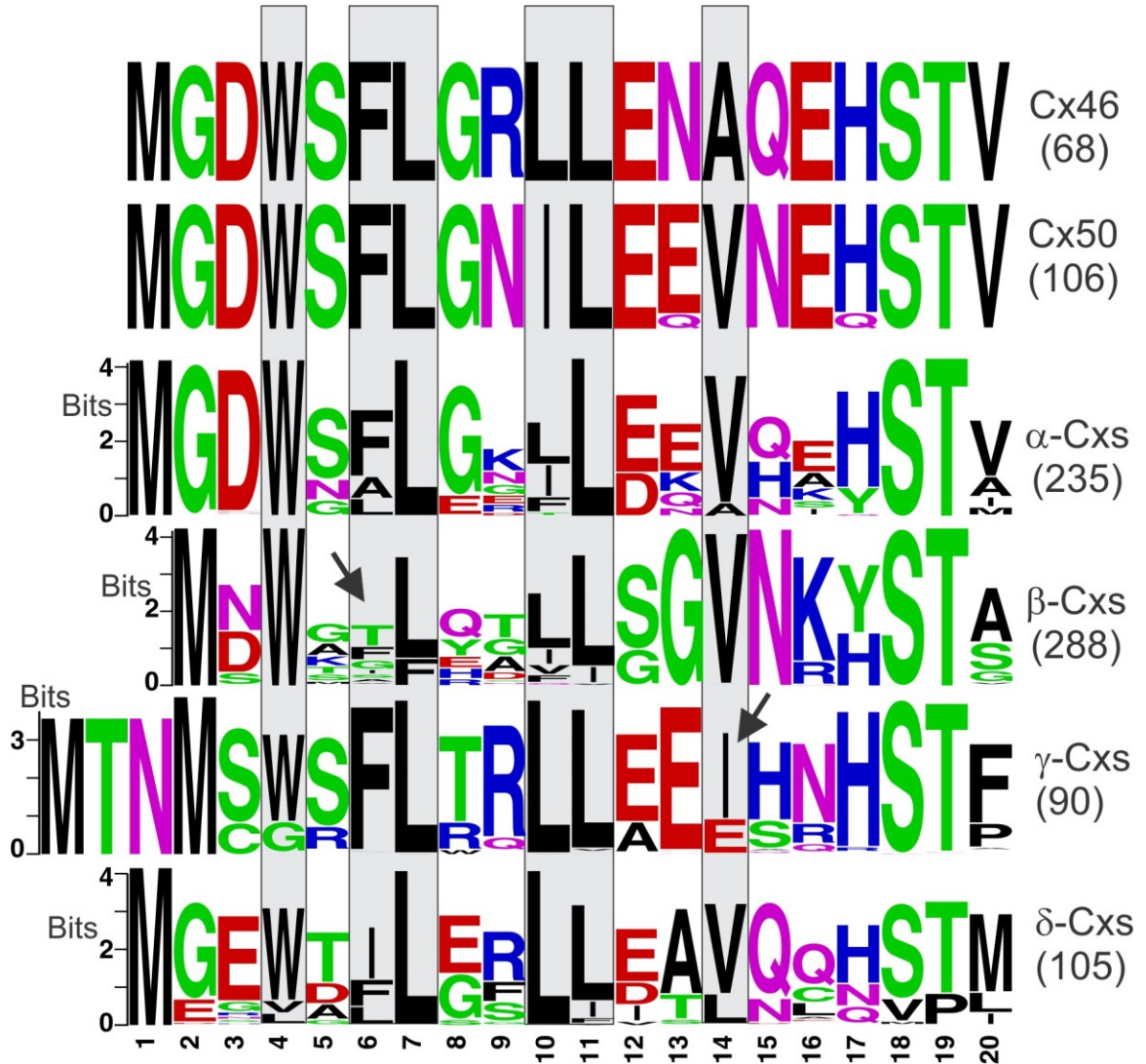


**Figure 3-2:** Sequence logos of the first 20 amino acid residues in the amino terminal domains (left hand is the beginning of amino terminus) of Cx46, Cx50, and their orthologs are shown. These logos are also aligned with logos of a collection of alpha,

beta, gamma, and delta connexins. The NT  $\alpha$ -helix structure (cartoon view) and the hydrophobic residues in this part of the NT domain are shown as stick view. As shown in these aligned logos the hydrophobic residues are highly conserved and in the hydrophobic residue equivalent positions (grey boxes), nearly all connexin families also have hydrophobic residues. Number of each group connexins included in creating the logos is indicated. WebLogo was used to generate connexin logos (Crooks et al., 2004).

In addition to hydrophobic residues of NT domain, we also explored the functional role of other residues on 13<sup>th</sup> and 15<sup>th</sup> positions. As mentioned earlier, there are several amino acid residue differences between the NT domains of Cx46 and Cx50 (Fig 3-1). The 13<sup>th</sup> position is interesting as the two corresponding residues are different in charge properties. This position also faces the pore entrance. Cx46 N13E was predicted to have increased  $\gamma_j$  because previous studies observed a direct correlation between net negative charge of NT domain and  $\gamma_j$  (Xin and Bai, 2013). However, other factors such as intra- or inter-subunit interactions with other domains could play crucial role in determining  $\gamma_j$ . Introduced glutamic acid residue is possibly interacting with neighboring R9 residue forming salt bridge interactions as suggested by our homology model (see Fig.2-10A). Bulkier glutamic acid could also impede the passage of substrates through the channel. Together, A14V and N13E might be responsible for the observed loss of function in Cx46-50NT observed in our previous study (Yue et al., 2021).

Cx50-46NT chimera GJ displayed single channel conductance of 116 pS, which is comparable to that of Cx50-N9R variant (122 pS). Thus, the 9<sup>th</sup> residue seems to play a critical role in determining the  $\gamma_j$  of Cx50-46NT and was responsible for most of the change in  $\gamma_j$  of the chimera as compared to wildtype (Yue et al., 2021). However, partial role of other residues cannot be ruled out. Our data showed that Cx50 E13N also decreased  $\gamma_j$  significantly to around 88% of wildtype conductance. Switching the negatively charged glutamate to polar uncharged asparagine results in decreased negative electrostatic charge of NT domain in each connexin. This can be delineated as Cx50 is a cation preferred channel, negatively charged residues can attract cations locally to facilitate cations movement through GJ channel pore thereby increasing rate of permeation (Srinivas et al., 1999). Charged residues of the NT domain have been shown

to determine the  $V_j$ -gating polarity, and affecting  $V_j$  sensing in Cx40, Cx50, Cx26, and Cx32 (Musa et al., 2004, Peracchia and Peracchia, 2005, Purnick et al., 2000, Verselis et al., 1994, Oh et al., 2004). Cx50 N15Q also decreased  $\gamma_j$  to 74% of wildtype  $\gamma_j$  as bulkier glutamine might interfere with normal stabilizing interactions with the opposing M1 domain. Table 3-1 summarizes key functional differences between each variant and its corresponding wildtype. Collectively, our functional characterization of individual variants suggests that a major contribution from the 9<sup>th</sup> position alongside partial roles of 13<sup>th</sup> and 15<sup>th</sup> positions are responsible for the observed decreased unitary conductance of Cx50-46NT chimera.

**Table 3-1:** Summary of functional changes observed in each variant as compared to corresponding Cx46 or Cx50 wildtypes.

<b>Variant/ Wildtype</b>	<b>Coupling%</b>	<b>G<sub>j</sub> (nS)</b>	<b><math>\gamma_j</math> (pS)</b>	<b>Comments</b>
<b>Cx46</b>	59 ± 20	4.85 ± 8.09	192 ± 5	
L10I	Statistically similar to wildtype			Loss of gating on one $V_j$ polarity, steric clash with L90
N13E	47% decrease (31 ± 21%)*	99% decrease (0.039 ± 0.38)***	52% decrease (93 ± 17)**	Occasional salt bridge interaction with R9
A14V	Statistically similar to wildtype	84% decrease (0.77 ± 0.60)**	51% decrease (94 ± 11)***	Steric clash with T89

Q15N	Statistically similar to wildtype			
<b>Cx50</b>	64 ± 27	2.84 ± 3.07	220 ± 7	
I10L	Statistically similar to wildtype			
E13N	Statistically similar to wildtype	27% decrease (2.07 ± 2.24)**	12% decrease (193 ± 17)*	Decreased net negative charge of NT domain
V14A	Statistically similar to wildtype			
N15Q	Statistically similar to wildtype	55% decrease (1.28 ± 1.48)*	26% decrease (162 ± 14)**	Glutamine is bulkier than asparagine
S89T	Failed to form functional GJs			

G<sub>j</sub>, Coupling conductance; γ<sub>j</sub>, single channel conductance. \*p < 0.05, \*\*p < 0.01, \*\*\*p < 0.001.

### 3.4 Comparison among human, sheep, and mouse lens GJs

Although the eye lens connexins: Cx43, Cx46, and Cx50 are expressed in many different animal species, sequence and function of each connexin are often very similar (Mathias et al., 2010). Sheep and human Cx46 share 67% of overall sequence identity while mouse and sheep are 65% identical overall. In structurally resolved residues, sCx46 and hCx46 or

mCx46 share around 95-96% sequence identity in the residues 2-109, and 94% in residues 137-224. Cx50 has higher sequence identity among different species as sCx50 and hCx50 or mCx50 share approximately 85-87% overall identity and 95-97% sequence identity over resolved structural domains (2-109 and 149-236). Interestingly, despite the small differences noticed in sequence alignment of structurally resolved areas, there are some observed differences in channel properties of GJs among sheep and human or mouse. To illustrate, our data showed that sCx46 have a  $\gamma_j = 192$  pS. Previous study showed 166 pS or the same sheep connexin (Ye et al., 2019). Data on rat Cx46 showed  $\gamma_j$  that range from  $140 \pm 8$  pS in CsCl-based intracellular solution (ICS) (Hopperstad et al., 2000), and 213-300 pS in KCl-based ICS (Trexler et al., 2000, Sakai et al., 2003). Data on  $\gamma_j$  of human Cx46 homotypic GJs are limited. One study reported  $\gamma_j$  of  $\sim 140$  pS for hCx46, although in a small number of cases larger openings were seen ( $\sim 180$  pS) (Abrams et al., 2018). In our lab, hCx46 was unable to form functional GJs in N2A cells and impossible to study. Mouse and human Cx50 recorded conductance ranging from 200-220 pS (Tong et al., 2015, Srinivas et al., 1999, Rubinos et al., 2012, Xin et al., 2010). Our present study, using CsCl-based ICS, displayed unitary conductance in the same range as those of rat or human Cx46 or Cx50  $\gamma_j$ s. Other factors, including small differences in the ICS component, experimental procedures, experimenter habits, etc. could also play a role in the observed differences in  $\gamma_j$ . In addition, our data showed that sCx46 have a  $\gamma_j = 192$  pS which is significantly lower than that of sCx50 (220 pS). Similarly, previous study showed similar relationship between the two sheep connexins: 166 pS vs 208 pS (Yue et al., 2021).

### 3.5 Limitations and future studies

Previous experiments in our laboratory showed too low coupling% of hCx46 in N2A cells to obtain any reliable data. We tried to switch to another model cell line, HeLa cells, only found that HeLa cells often showed endogenous coupling due to possibly expression of an endogenous connexin, making it impossible to obtain consistent data for our designed experiments. These findings limit our ability for comparable functional studies on human lens connexins.

It would be interesting to follow-up with Cx50 S89T and design Cx50 S89T fusion tagged with GFP to perform localization studies in order to explore possible reasons for the loss of function of this variant. We expect that the ‘mirror’ variant, Cx46 T89S, will form GJs with no major functional changes, as there is no steric clash in our structure model (Fig. 2-10). However, the decrease in the side chain length of both S89 and approximate A14 might result in more close hydrophobic packing pushing NT away from the pore core possibly increasing pore diameter compared to wildtype, so it is still interesting to investigate its channel properties and compare it to Cx50 S89T.

To quantitatively analyze open dwell time for the main open state could be used in the future to determine open state stability. Future studies on MD simulations to obtain structural insights on each variant GJ in a dynamic setting, gating kinetics, or ion/substrate selectivity of these channels would be also interesting. Functional characterization of double or triple point variants, such as Cx46 NA (Double mutation composed of N13E and A14V) or Cx46 LNA (Triple mutation composed of L10I, N13E, and A14V) would provide further understanding of mechanistic determinants of channel function. We expect that at least one of these two variants will form nonfunctional GJs. Another interesting triple variant would be Cx50 NEN (Including N9R, E13N, and N15Q). Depending on our functional analysis, we expect this variant would be nonfunctional too.

### 3.6 Summary

Previous functional studies have established a critical role for NT domain in determining channel properties. Despite that Cx46 and Cx50 share around 80% sequence identity and 92% sequence similarity over resolved structural domains, they are different in  $\gamma_j$ . To dissect the molecular determinants behind this difference, we aligned the amino acid sequence which shows five key different residues at positions: 9<sup>th</sup>, 10<sup>th</sup>, 13<sup>th</sup>, 14<sup>th</sup> and 15<sup>th</sup> positions and designed point variants where one amino acid residue was switched between Cx46 and Cx50. In Cx46, 13<sup>th</sup> and 14<sup>th</sup> positions (N13E and A14V) changed  $\gamma_j$  drastically to around 48% and 49% of wildtype  $\gamma_j$ , respectively, and also decreased coupling% and coupling conductance compared to wildtype GJs. Homology structure



model of A14V indicates steric clash between A14 and T89 on M2 domain. To further clarify the role of this steric clash, we designed and functionally characterized Cx50 S89T mutant which was unable to form functional channel beside steric clash demonstration on the homology model of this variant. Cx46 L10I changed  $V_j$ -gating partially. Q15N was similar to wildtype in coupling conductance,  $V_j$ -gating, and rate of ion permeation. For Cx50, E13N and N15Q resulted in small but significant decrease in  $\gamma_j$  compared to wildtype. In addition, they decreased coupling conductance. 10<sup>th</sup> and 14<sup>th</sup> variants didn't affect the function of Cx50 GJ. Overall, our functional data and homology models indicate packing interactions between hydrophobic residues of NT and other residues in M2 domain are important for their  $V_j$ -gating and  $\gamma_j$  in these and possibly other GJs.

### 3.7 References

- ABRAMS, C. K., PEINADO, A., MAHMOUD, R., BOCARSLY, M., ZHANG, H., CHANG, P., BOTELLO-SMITH, W. M., FREIDIN, M. M. & LUO, Y. 2018. Alterations at Arg(76) of human connexin 46, a residue associated with cataract formation, cause loss of gap junction formation but preserve hemichannel function. *Am. J. Physiol. Cell Physiol.*, 315, C623-c635.
- BARGIELLO, T. A., OH, S., TANG, Q., BARGIELLO, N. K., DOWD, T. L. & KWON, T. 2018. Gating of Connexin Channels by transjunctional-voltage: Conformations and models of open and closed states. *Biochim Biophys Acta Biomembr*, 1860, 22-39.
- BEZANILLA, F. 2000. The voltage sensor in voltage-dependent ion channels. *Physiol. Rev.*, 80, 555-92.
- CROOKS, G. E., HON, G., CHANDONIA, J. M. & BRENNER, S. E. 2004. WebLogo: a sequence logo generator. *Genome Res.*, 14, 1188-90.
- FLORES, J. A., HADDAD, B. G., DOLAN, K. A., MYERS, J. B., YOSHIOKA, C. C., COPPERMAN, J., ZUCKERMAN, D. M. & REICHOW, S. L. 2020. Connexin-46/50 in a dynamic lipid environment resolved by CryoEM at 1.9 Å. *Nat Commun*, 11, 4331.
- HANSEN, L., YAO, W., EIBERG, H., FUNDING, M., RIISE, R., KJAER, K. W., HEJTMANCIK, J. F. & ROSENBERG, T. 2006. The congenital "ant-egg" cataract phenotype is caused by a missense mutation in connexin46. *Mol. Vis.*, 12, 1033-9.
- HOPPERSTAD, M. G., SRINIVAS, M. & SPRAY, D. C. 2000. Properties of gap junction channels formed by Cx46 alone and in combination with Cx50. *Biophys. J.*, 79, 1954-66.
- JAMSHEER, A., WISNIEWSKA, M., SZPAK, A., BUGAJ, G., KRAWCZYNSKI, M. R., BUDNY, B., WAWROCKA, A. & LATOS-BIELEŃSKA, A. 2009. A novel GJA1 missense mutation in a Polish child with oculodentodigital dysplasia. *J Appl Genet*, 50, 297-9.
- JAVADIYAN, S., LUCAS, S. E. M., WANGMO, D., NGY, M., EDUSSURIYA, K., CRAIG, J. E., RUDKIN, A., CASSON, R., SELVA, D., SHARMA, S., LOWER, K. M., MEUCKE, J. & BURDON, K. P. 2018. Identification of novel mutations causing pediatric cataract in Bhutan, Cambodia, and Sri Lanka. *Mol Genet Genomic Med*, 6, 555-64.

- KELLY, S. C., RATAJCZAK, P., KELLER, M., PURCELL, S. M., GRIFFIN, T. & RICHARD, G. 2006. A novel GJA 1 mutation in oculo-dento-digital dysplasia with curly hair and hyperkeratosis. *Eur. J. Dermatol.*, 16, 241-5.
- LIU, X. Z., XIA, X. J., ADAMS, J., CHEN, Z. Y., WELCH, K. O., TEKIN, M., OUYANG, X. M., KRISTIANSEN, A., PANDYA, A., BALKANY, T., ARNOS, K. S. & NANCE, W. E. 2001. Mutations in GJA1 (connexin 43) are associated with non-syndromic autosomal recessive deafness. *Hum. Mol. Genet.*, 10, 2945-51.
- MACKAY, D. S., BENNETT, T. M., CULICAN, S. M. & SHIELS, A. 2014. Exome sequencing identifies novel and recurrent mutations in GJA8 and CRYGD associated with inherited cataract. *Hum Genomics*, 8, 19.
- MATHIAS, R. T., WHITE, T. W. & GONG, X. 2010. Lens gap junctions in growth, differentiation, and homeostasis. *Physiol. Rev.*, 90, 179-206.
- MUSA, H., FENN, E., CRYE, M., GEMEL, J., BEYER, E. C. & VEENSTRA, R. D. 2004. Amino terminal glutamate residues confer spermine sensitivity and affect voltage gating and channel conductance of rat connexin40 gap junctions. *J. Physiol.*, 557, 863-78.
- MYERS, J. B., HADDAD, B. G., O'NEILL, S. E., CHOREV, D. S., YOSHIOKA, C. C., ROBINSON, C. V., ZUCKERMAN, D. M. & REICHOW, S. L. 2018. Structure of native lens connexin 46/50 intercellular channels by cryo-EM. *Nature*, 564, 372-377.
- OH, S., RIVKIN, S., TANG, Q., VERSELIS, V. K. & BARGIELLO, T. A. 2004. Determinants of gating polarity of a connexin 32 hemichannel. *Biophys. J.*, 87, 912-28.
- PAZNEKAS, W. A., BOYADJIEV, S. A., SHAPIRO, R. E., DANIELS, O., WOLLNIK, B., KEEGAN, C. E., INNIS, J. W., DINULOS, M. B., CHRISTIAN, C., HANNIBAL, M. C. & JABS, E. W. 2003. Connexin 43 (GJA1) mutations cause the pleiotropic phenotype of oculodentodigital dysplasia. *Am. J. Hum. Genet.*, 72, 408-18.
- PAZNEKAS, W. A., KARCZESKI, B., VERMEER, S., LOWRY, R. B., DELATYCKI, M., LAURENCE, F., KOIVISTO, P. A., VAN MALDERGEM, L., BOYADJIEV, S. A., BODURTHA, J. N. & JABS, E. W. 2009. GJA1 mutations, variants, and connexin 43 dysfunction as it relates to the oculodentodigital dysplasia phenotype. *Hum. Mutat.*, 30, 724-33.
- PERACCHIA, C. & PERACCHIA, L. L. 2005. Inversion of both gating polarity and CO<sub>2</sub> sensitivity of voltage gating with D3N mutation of Cx50. *Am. J. Physiol. Cell Physiol.*, 288, C1381-9.

- PORNTAVEETUS, T., SRICHOMTHONG, C., OHAZAMA, A., SUPHAPEETIPORN, K. & SHOTELERSUK, V. 2017. A novel GJA1 mutation in oculodentodigital dysplasia with extensive loss of enamel. *Oral Dis.*, 23, 795-800.
- PURNICK, P. E., OH, S., ABRAMS, C. K., VERSELIS, V. K. & BARGIELLO, T. A. 2000. Reversal of the gating polarity of gap junctions by negative charge substitutions in the N-terminus of connexin 32. *Biophys. J.*, 79, 2403-15.
- RUBINOS, C., SÁNCHEZ, H. A., VERSELIS, V. K. & SRINIVAS, M. 2012. Mechanism of inhibition of connexin channels by the quinine derivative N-benzylquininium. *J. Gen. Physiol.*, 139, 69-82.
- SAKAI, R., ELFGANG, C., VOGEL, R., WILLECKE, K. & WEINGART, R. 2003. The electrical behaviour of rat connexin46 gap junction channels expressed in transfected HeLa cells. *Pflugers Arch.*, 446, 714-27.
- SRINIVAS, M., COSTA, M., GAO, Y., FORT, A., FISHMAN, G. I. & SPRAY, D. C. 1999. Voltage dependence of macroscopic and unitary currents of gap junction channels formed by mouse connexin50 expressed in rat neuroblastoma cells. *J. Physiol.*, 517 ( Pt 3), 673-89.
- TONG, J. J., SOHN, B. C., LAM, A., WALTERS, D. E., VERTEL, B. M. & EBIHARA, L. 2013. Properties of two cataract-associated mutations located in the NH2 terminus of connexin 46. *Am. J. Physiol. Cell Physiol.*, 304, C823-32.
- TONG, X., AOYAMA, H., SUDHAKAR, S., CHEN, H., SHILTON, B. H. & BAI, D. 2015. The First Extracellular Domain Plays an Important Role in Unitary Channel Conductance of Cx50 Gap Junction Channels. *PLoS One*, 10, e0143876.
- TONG, X., AOYAMA, H., TSUKIHARA, T. & BAI, D. 2014. Charge at the 46th residue of connexin 50 is crucial for the gap-junctional unitary conductance and transjunctional voltage-dependent gating. *J. Physiol.*, 592, 5187-202.
- TREXLER, E. B., BUKAUSKAS, F. F., KRONENGOLD, J., BARGIELLO, T. A. & VERSELIS, V. K. 2000. The first extracellular loop domain is a major determinant of charge selectivity in connexin46 channels. *Biophys. J.*, 79, 3036-51.
- VERSELIS, V. K., GINTER, C. S. & BARGIELLO, T. A. 1994. Opposite voltage gating polarities of two closely related connexins. *Nature*, 368, 348-51.
- XIN, L. & BAI, D. 2013. Functional roles of the amino terminal domain in determining biophysical properties of Cx50 gap junction channels. *Front. Physiol.*, 4, 373.
- XIN, L., GONG, X. Q. & BAI, D. 2010. The role of amino terminus of mouse Cx50 in determining transjunctional voltage-dependent gating and unitary conductance. *Biophys. J.*, 99, 2077-86.

- YE, Y., WU, M., QIAO, Y., XIE, T., YU, Y. & YAO, K. 2019. Identification and preliminary functional analysis of two novel congenital cataract associated mutations of Cx46 and Cx50. *Ophthalmic Genet.*, 40, 428-435.
- YUE, B., HADDAD, B. G., KHAN, U., CHEN, H., ATALLA, M., ZHANG, Z., ZUCKERMAN, D. M., REICHOW, S. L. & BAI, D. 2021. Connexin 46 and connexin 50 gap junction channel properties are shaped by structural and dynamic features of their N-terminal domains. *J. Physiol.*, 599, 3313-3335.
- ZHANG, L., LIANG, Y., ZHOU, Y., ZENG, H., JIA, S. & SHI, J. 2018. A Missense Mutation in GJA8 Encoding Connexin 50 in a Chinese Pedigree with Autosomal Dominant Congenital Cataract. *Tohoku J. Exp. Med.*, 244, 105-111.

## Curriculum Vitae

**Name:** Roa'a Jaradat

**Post-secondary Education and Degrees:** Jordan University of Science and Technology  
Irbid, Jordan  
2009-2015 PharmD

Jordan University of Science and Technology  
Irbid, Jordan  
2015-2017 MSc Clinical Pharmacy

The University of Western Ontario  
London, Ontario, Canada  
2020-2022 MSc

**Related Work Experience** Teaching Assistant- PHYSPHRM 3000E  
University of Western Ontario  
September 2020-December 2020

### Posters:

- **Research day 2020 - Department of Physiology and Pharmacology**

### Research day 2021 - Department of Physiology and Pharmacology

#### Publications:

- Jaradat, R., Lahlouh, A. and Mustafa, M., 2020. Sleep quality and health related problems of shift work among resident physicians: a cross-sectional study. *Sleep Medicine*, 66, pp.201-206.
- Jaradat, R., Lahlouh, A., Alshogran, O., Aldabbour, B. and Balusha, A., 2019. Nosocomial Infections among Patients with Intracranial Hemorrhage: A Retrospective Data Analysis of Predictors and Outcomes. *Clinical Neurology and Neurosurgery*, 182, pp.158-166.
- Mayyas, F., Jaradat, R. and Alzoubi, K. (2018). Cardiac effects of fish oil in a rat model of streptozotocin-induced diabetes. *Nutrition, Metabolism and Cardiovascular Diseases*, 28(6), pp.592-599.